



3D finite element modeling of bond-controlled behavior of steel and basalt FRP-reinforced concrete square bridge columns under lateral loading



Arafa M.A. Ibrahim^a, Mohamed F.M. Fahmy^{b,c}, Zhishen Wu^{a,*}

^a Dept. of Urban and Civil Engineering, Ibaraki University, 4-12-1 Nakanarusawa-cho, Hitachi 316-8511, Japan

^b International Institute for Urban Systems Engineering, Southeast University, Nanjing 210096 China

^c Dept. of Civil Engineering, Faculty of Engineering, Assiut University, Assiut 71516, Egypt

ARTICLE INFO

Article history:

Available online 7 January 2016

Keywords:

Bond
BFRP
Finite element model
Bridges
Columns
Lateral loading

ABSTRACT

Bond between reinforcing bars and concrete plays an important role in controlling the structural performance of reinforced concrete (RC) structures. The main objective of this study was to create and execute a detailed three dimensional (3D) finite element (FE) model evaluating the structural performance of fiber reinforced polymer (FRP)-steel RC (FSRC) bridge columns and considering the effect of several bond conditions between FRP bars and concrete. Hence, bond behavior of basalt FRP (BFRP) bars with different surface conditions was firstly discussed in comparison with ribbed steel bars. After that, results of the created 3D FE models for FSRC columns reinforced with BFRP bars having different bond conditions were validated in the light of results of four columns experimentally tested under the combined effect of constant axial load and cyclic lateral loading. Ultimately, a parametric study was conducted to find out the effect of different bond conditions of FRP bars on the structural performance of FSRC columns. The numerical results showed that response of FSRC columns to lateral loading is dependent on bond conditions between FRP bars and the surrounding concrete: characteristics of bond–slip relationship of FRP bars could be adopted as design parameters controlling the behavior of FSRC columns. Failure mode, lateral strength, post-yield stiffness ratio, ductility at the peak lateral strength and at failure are all depend on the bond parameters of FRP bars. However, FRP bond parameters did not show a pronounced impact on the column elastic stiffness.

© 2016 Elsevier Ltd. All rights reserved.

1. Introduction

Recently, fiber reinforced polymer (FRP) composites are receiving increased attention due to its superior performance compared to conventional steel [1]. Several experimental and numerical studies investigated application of FRP composites as reinforcing and strengthening material for reinforced concrete (RC) structures [2–5]. In general, the performance of RC structures depends not only on mechanical characteristics of concrete and reinforcement but also on the composite action between the two components [6,7]. This is the case for any type of reinforcement, including FRP composite materials [8,9]. Bond between concrete and reinforcing bars is mandatory to transfer the forces between both materials and thus it significantly affects the stiffness, strength, and ductility in addition to cracking behavior and the tension

stiffening of RC structures [10]. Moreover, bond between reinforcement and concrete directly influences deformation capacity and hence the length of plastic hinge, which is of importance for the rotation capacity of RC members [11]. Previous researches [12–14] provided basic understanding of the bond behavior of RC structures reinforced with conventional steel bars. For instance, experimental investigations on beam-column joints subjected to simulated earthquake loading indicated that the global response of these joints may be determined by the local bond response [15]. On the other hand, FRP composites are new materials with manifold shapes and properties, and they all behave differently in many contexts. To adopt FRP composites as reinforcement for modern constructions, these materials must be brought to the codes of practice [16]. Therefore, bond behavior between FRP bars and the surrounding materials is a fundamental aspect in evaluating the structural performance of FRP-RC structures.

In contrast to steel reinforcing bars, the unique characteristics of every FRP material and the wide variety of fiber/resin interfaces

* Corresponding author. Tel.: +81 294 38 5179; fax: +81 294 38 5268.

E-mail address: zhishen.wu.prof@vc.ibaraki.ac.jp (Z. Wu).

as well as surface configurations made the bond behavior of FRP bars hard to be standardized [17]. Considerable research efforts have been done to describe the bond behavior of FRP bars in concrete as summarized by [17–20]. Experimental and numerical studies on RC beams reinforced by different types of FRP bars demonstrated a great influence of FRP bond–slip mechanism on the flexural behavior of RC beams [21]. It is also established that bond between FRP bars and concrete depends on several parameters such as concrete strength, bar diameter, bar surface treatment, embedment length, and concrete confinement [22–24]. Among these parameters, it has been emphasized that bond is strongly dependent on the surface characteristics of the FRP bar and its treatment (ribbed, braided, indented, or sand coated). For example, Cosenza et al. [25] concluded that bond strengths for the ribbed and indented FRP bars are comparable to those obtained for deformed steel bars, but they are lower than the bond strength of sand-coated bars. Similarly, Hao et al. [26] observed that the increase in the rib spacing or the decrease in the rib height of glass FRP (GFRP) ribbed bars of 10-mm diameter, up to certain limits, leads to a decrease in both the peak bond strength and the corresponding slip. Besides the significance influence of surface conditions, many researchers have reported that bond strength of FRP bars is inversely proportional to the bar diameter [23,24].







Recent advances in earthquake engineering favor performance-based approaches for the seismic design of modern concrete bridges located in active seismic zones. To ensure the required recoverability of modern bridge columns, unbonded-prestressed strands [27–29] and shape memory alloy [30] have been examined. Wu et al. [31] proposed steel-FRP composite bar (SFCB) to combine the advantages of mechanical and physical properties of both steel and FRP composites: high elastic modulus and good ductility of common steel bar and good anti-corrosion ability and elasticity of FRP composites. Reinforcing RC bridge columns with this composite bar could guarantee the required post-earthquake recoverability, whereby residual column deformation and post-yield stiffness could be controlled. Ibrahim et al. [32] proposed combination of steel and FRP composites as a reinforcement for FRP-RC damage-controllable bridge columns. Experimental tests on seven columns were carried out under the effect of constant axial load and reversed cyclic lateral loads to examine the performance of the proposed system: five scaled concrete bridge columns reinforced by steel and FRP composites (FSRC columns) and two steel-RC (SRC) columns. Along with the observed stable post-yield stiffness (hardening behavior) and high column deformability before encountering strength degradation, bond condition of the FRP bars to the surrounding concrete had pronounced effects on the column failure mode, post-yield stiffness, residual displacement, and ductility.

Analysis of FSRC columns would be a challenging problem and the existence of FRP bars with different bond conditions could certainly increase its complexity. Bond behavior and its influence on the structural performance are very difficult to be fully examined through only experimental studies. Hence, an appropriate and consistent numerical approach for the analysis and prediction of the performance of such structures is still required. Hence, the main objective of this study was to create a three dimension (3D) finite element (FE) model for FSRC columns that is able to simulate the structural performance of bond-controlled FSRC columns. Hence, three subsequent sections are presented in this paper as follows: (1) the first section addresses the bond behavior of BFRP bars with different surface conditions; (2) a 3D FE model for FSRC columns using the FE ANSYS code version 13 [33] was created and validated in the second section in the light of test results of concrete columns reinforced with steel and BFRP bars with different bond conditions as well as experimental results of one SRC column; (3) the last section presents a general bond-based numerical study on FSRC column model using the verified FE approach.

2. Bond–slip behavior of BFRP bars with different surface conditions

Recently, basalt FRPs (BFRPs) have been emerged as a promising alternative to conventional FRPs in reinforcing concrete structures [17]. BFRP has been proven to show advantageous characteristics in mechanical, chemical, working temperatures, and high ratio of performance to cost in comparison to other FRPs. So, Ibrahim et al. [32] proposed BFRP bars for application in the FSRC system. In the study of Ibrahim et al. [34], bond–slip behavior between BFRP bars and concrete was examined through pull-out tests on 10-mm-diameter BFRP bars with five different surface conditions. To represent the local bond stress–slip relationship of the tested bars, Ibrahim et al. [34] showed that the well-known BPE bond–slip model [35] can be applied. Table 1 summarizes the parameters (τ_1 , S_1 , S_2 , K_d , and τ_2) of the optimized bond stress–slip behavior of all bars; τ_1 is the peak bond stress, S_1 is the corresponding slip, S_2 is the slip at the end of the horizontal plateau zone, K_d is the slope of the descending branch, and τ_2 is the residual bond stress (see Fig. 1a). Designation of these samples here are B10-S, B10-SH10, B10-SH5, B10-DH10, and B10-DI; where B refers to basalt, 10 is bar diameter and S, SH10, SH5, DH10 and DI are abbreviations for different surface conditions. S represents BFRP bar characterized by very small indentations (i.e., named in all parts of this study smooth BFRP bar); SH10 and SH5 are single strand helically wrapped around the smooth BFRP bar with pitch of 10 mm and 5 mm, respectively; DH10 is double helically wrapped smooth BFRP bars with 10 mm pitch; and DI is BFRP bars with deeply

Table 1
Details and bond–slip model parameters of BFRP and steel bars.

Bar ID	Surface condition	Parameters of the bond–slip model					
		τ_1 (MPa)	S_1 (mm)	S_2/S_1	K_d (MPa/mm)	τ_2/τ_1	α
S10		12.1	1.0	2.0	2.05	0.3	0.4
B10-S		7.2	1.1	2.0	0.60	0.5	0.5
B10-SH10		10.9	1.7	1.7	0.74	0.55	0.5
B10-SH5		11.2	0.9	4.0	0.78	0.50	0.5
B10-DH10		12.2	2.2	1.6	0.85	0.50	0.5
B10-DI		12.5	1.4	1.2	1.20	0.45	0.6

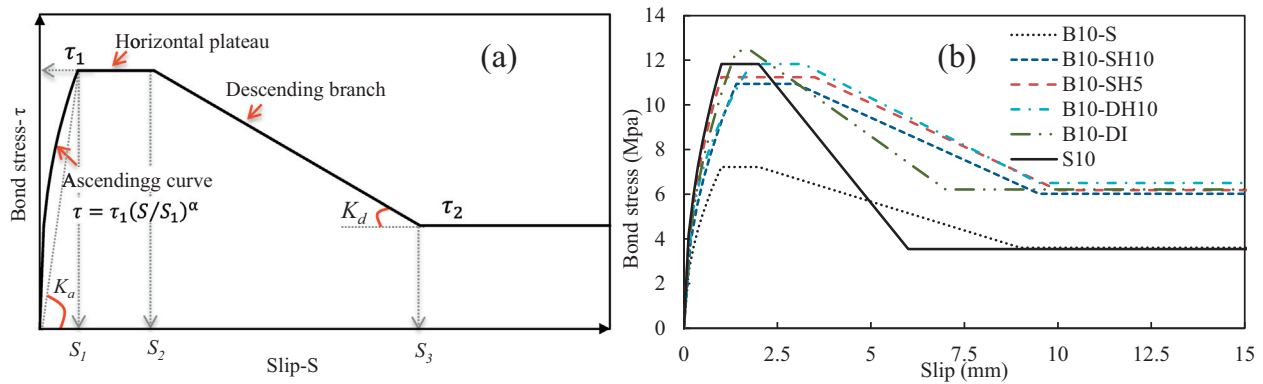


Fig. 1. (a) Local bond-slip model of FRP bars [35] and (b) bond-slip models of ribbed steel and BFRP bars with different surface conditions [34].

Table 2

Mechanical properties of steel and FRP materials.

Material type	Elastic modulus E (GPa)	Yield stress f_y (MPa)	Tensile strength f_u (MPa)
13-mm-diameter steel bars	200	375	560
10-mm-diameter steel bars	200	360	550
6-mm-diameter steel bars	200	400	625
10-mm-diameter BFRP bars	48.1	–	1113
6-mm-diameter BFRP bars	47.5	–	1345
BFRP sheet	91	–	2100

ribbed surface. Details of the surface conditions of the five bars are shown in Table 1. For comparison, another pull-out test was carried out on a ribbed steel bar (S10) with approximately the same diameter of the BFRP bars and test results are presented in Table 1. Material properties of the BFRP and steel bars are listed in Table 2 and average concrete compressive strength of the pull-out test specimens on the day of test was 35 MPa. Detailed description of the pull-out tests can be found elsewhere, Ibrahim et al. [34].

The characterized bond-slip relationships of the BFRP and steel bars could be modeled as shown in Fig. 1b. Compared to steel bar, Fig. 1b shows that the smooth BFRP bar possesses much lower bond strength and lower stiffness for the ascending branch. When surface of BFRP bar (B10-S) was altered to rough condition in the other samples, not only the bond strength but also the stiffness of the ascending branch can be improved to a level comparable to that of the steel bar. Moreover, slopes of the descending branches of all BFRP bars are softer than that of the steel bar. This characteristic would be favored in seismic design as it could allow FSRC structures dissipate more energy. It should be noted that slopes of the descending branch of all treated BFRP bars are comparable except the last sample which showed a steeper slope, however, it was still lower than that of the steel bar.

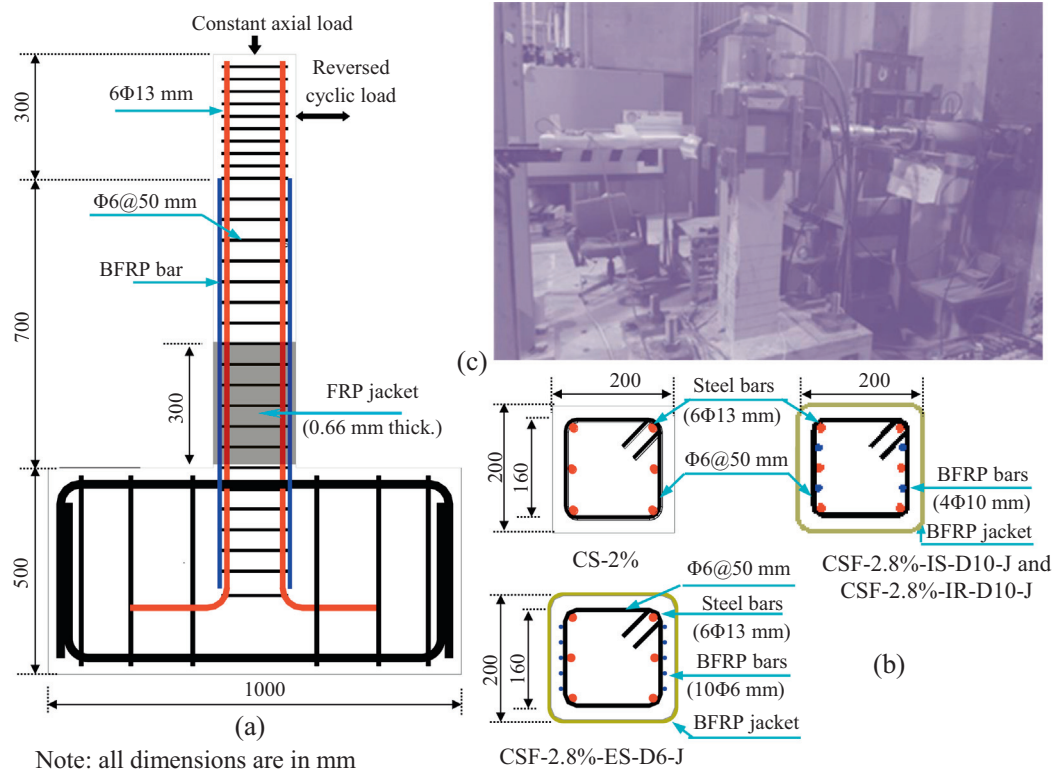
3. Finite element modeling of SRC and FSRC columns

3.1. Bond-controlled FSRC columns (experimental results)

Cyclic responses of FSRC columns in comparison with SRC columns were presented in the study of Ibrahim et al. [32]. Here, a summary for test results of two FSRC columns and one SRC column are presented. In addition, results of a new FSRC column was tested under the effect of constant axial load and several excursions of lateral loading are also addressed. All specimens were one-sixth scale columns and, as shown in Fig. 2, had square cross-section of 200-mm-edge length, height to the point of lateral load application of 850 mm, and a deep heavily reinforced concrete base of $1.0 \times 0.5 \times 0.5$ m (length \times width \times depth). In all specimens, steel reinforcements consisted of six longitudinal ribbed steel bars of

13-mm-diameter, which corresponds to 0.02 times the gross-section area of the column, and 6-mm-diameter stirrups placed at intervals of 50 mm. Designation of the FSRC columns tested by Ibrahim et al. [32] were CSF-2.8%-IS-D10-J and CSF-2.8%-IR-D10-J and the SRC column was named CS-2%. In addition to the steel reinforcements, the two FSRC specimens were reinforced with two 10-mm-diameter BFRP bars placed on each of two opposite sides of the columns (those with the highest tension/compression) at the same place as the longitudinal steel bars. The BFRP bars were extended to a height of 700 mm from the column base and embedded in the column footing to a depth of 300 mm. By summing the area of steel and BFRP bars, the resultant longitudinal reinforcement ratio became approximately 2.8%. BFRP bars with two different surface conditions were adopted in the FSRC columns, where the smooth (B10-S) and roughened (B10-DH10) BFRP bars (see Table 1) were used in the columns CSF-2.8%-IS-D10-J and CSF-2.8%-IR-D10-J, respectively. The new tested FSRC column was designated as CSF-2.8%-ES-D6-J, in which the longitudinal FRP reinforcement was five 6-mm-diameter smooth BFRP bars placed on each of the two opposite sides of the columns (those with the highest tension/compression) outside of the steel stirrups, i.e., in the concrete cover. Two reasons were attributed to placing the FRP bars in the concrete cover. The first reason was to prevent any concreting problems due to reinforcement congestions of large number of steel and FRP bars and the other was to create outside insulation walls together with the concrete covers that may help in preventing the moisture to reach the internal steel reinforcement and cause corruptions. By reinforcing the column with the above mentioned bars, the ratio of the longitudinal reinforcement becomes approximately the same as that of the previously mentioned FSRC columns (i.e., 2.8% of the gross-section area of the column). It is noteworthy that to increase the shear strength and ensure a ductile failure of all the FSRC columns, 0.666-mm-thickness BFRP jacket was provided to the plastic hinge region of the columns (i.e., the lowest 300-mm portion above the column base).

Properties of steel and FRP reinforcements and characteristics of the column specimens were summarized in Tables 2 and 3, respectively. For all columns, the loading procedure was as follows: first, an



Note: all dimensions are in mm

Fig. 2. Details of experimental columns: (a) column geometry and reinforcement, (b) cross-sections, and (c) test set-up.

Table 3
Details of experimental columns.

Specimen	f'_c (MPa)	Steel reinforcement		BFRP reinforcement			ρ_l %	
		Main	Lateral	Bars	Bars' surface	Bars' location		Jacket thickness
CS-2%	27.8	6Φ13	Φ6@50 mm	N/A			2.0	
CSF-2.8%-IS-D10-J	41.2	6Φ13	Φ6@50 mm	4Φ10	Smooth (B10-S)	Internal	0.666 (mm)	2.8
CSF-2.8%-IR-D10-J	32.9	6Φ13	Φ6@50 mm	4Φ10	Roughened (B10-DH10)	Internal	0.666 (mm)	2.8
CSF-2.8%-ES-D6-J	36.0	6Φ13	Φ6@50 mm	10Φ6	Smooth	External	0.666 (mm)	2.8

axial load of 40 kN was applied. Several excursions of lateral cyclic displacements were then applied based on the displacement at yielding of the SRC column (Δy). The lateral displacement sequence started with two cycles of $0.5\Delta y$ followed by two cycles of Δy and then three cycles each of $2\Delta y$, $3\Delta y$, $4\Delta y$, $6\Delta y$, $8\Delta y$, and $10\Delta y$ until failure.

The lateral load versus drift ratio relationships of the four column specimens are presented in Fig. 3. The lateral drift ratio was defined as the ratio of the lateral displacement at the point of the lateral load application of each column to the effective height of the column (850 mm). Values of the displacement ductility factor, μ , at different characteristic points were superimposed on the hysteretic responses, where $\mu = \delta/\delta_y$ and δ = lateral displacement at the load application point and δ_y = displacement at first steel yielding. As shown in Fig. 3a, failure of the conventionally steel reinforced column CS-2% was initiated by spalling of concrete cover and then buckling of the main reinforcement at displacement ductility of 10.3. That is the applied design strategy of steel reinforcement details was successful to reach a ductility of 8.8 without any substantial degradation in column strength. On the other hand, failure of the column CSF-2.8%-IS-D10-J was characterized by slippage of FRP bars from the surrounding concrete, which could be obviously realized from the induced strain in the FRP bars. Two considerable drops in the lateral strength occurred due to bond failure while loading this column at ductility of 8.1 and 9.5,

respectively, as shown in Fig. 3b. After that, rupture of steel bars occurred at a ductility of 10.8. Prior to bond failure, recorded results showed that the maximum strain in the BFRP bars at 50 mm above the column base was about 60% of the maximum strain capacity of the BFRP bars. For the column CSF-2.8%-IR-D10-J, roughening the surface of BFRP bars resulted in a significant enhancement in the bond condition between FRP bars and concrete, however this caused a sudden rupture of the BFRP bars at the column base after fulfilling a displacement ductility of 11.3 (Fig. 3c), at which time the strain in FRP bars at 150 mm above column base was over 70% of the BFRP rupture strain. From the lateral strength point of view, the column CSF-2.8%-IS-D10-J (i.e., with bond failure mode) and the columns CSF-2.8%-IR-D10-J (i.e., with FRP rupture failure mode) attained lateral strengths of approximately 1.54 and 1.7 times that of the SRC column, respectively. More discussion of the experimental results and the effect of surface texture configuration of the BFRP bars on the cyclic response of the two FSRC columns can be found in Ibrahim et al. [32].

Fig. 3d shows the response of CSF-2.8%-ES-D6-J column, and the column was able to continue carrying load up to a lateral drift of 4.6% ($\mu = 6.4$) to achieve average lateral strength of 62 kN. During loading the column to the second and third cycles of the same drift, a popping sound was heard and it was accompanied by a 10% drop in the column lateral strength. The recorded strain of

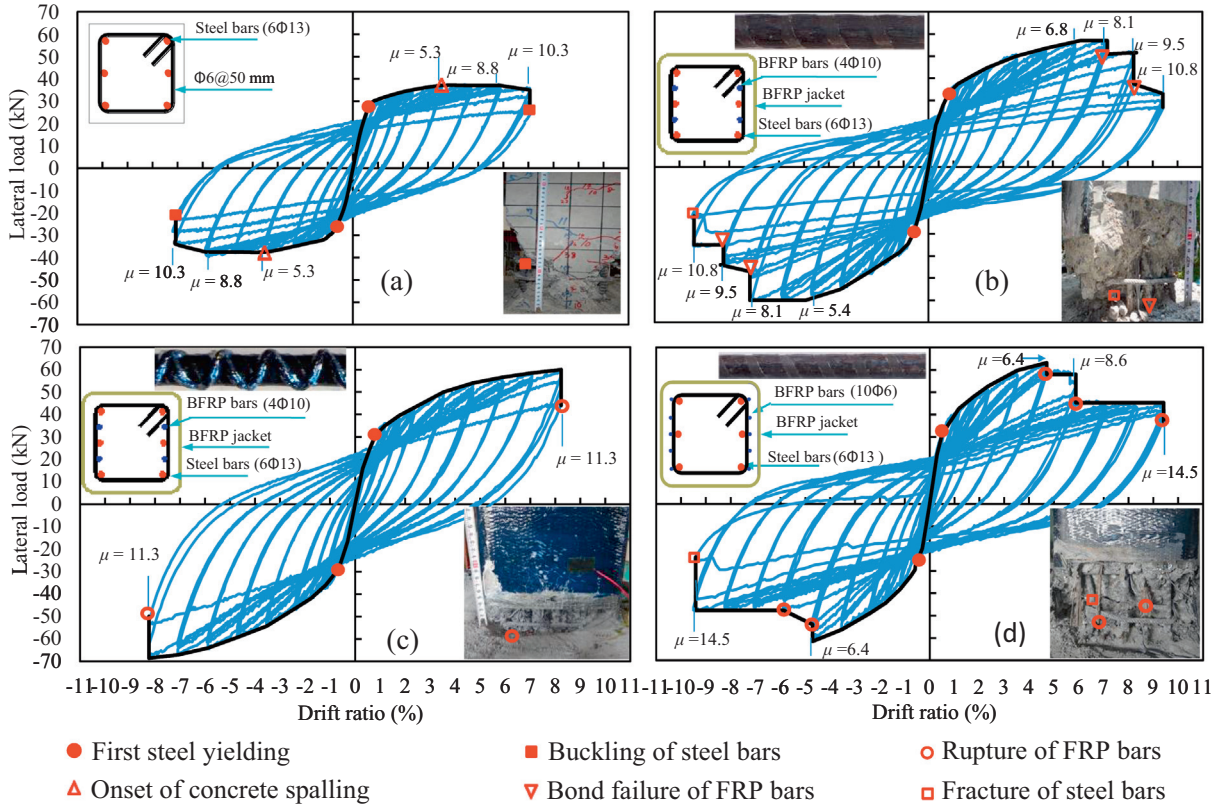


Fig. 3. Cyclic response of SRC and bond-controlled FSRC columns.

the intermediate BFRP bar at the column-footing interface, at this level of lateral drift, was approximately 80% of the rupture uniaxial strain. Actually, bond development of FRP reinforcing bars significantly depends on the bar diameter and concrete confinement [22–24]. So, this popping sound could be attributed to rupture of one or both corner BFRP bars, which located in the highly confined zone and could have a better bond behavior than 10-mm BFRP bars with similar texture condition. At a lateral drift of 5.9% ($\mu = 8.6$), rupture of the intermediate BFRP bars could be recognized by hearing another popping sound that was followed by approximately 16% drop in the column lateral strength. At this ductility level, the maximum strain recorded in the intermediate BFRP bars at 50 mm above the column base was approximately 85% of the ultimate axial strain.

In conclusion, the experimental results of the aforementioned FSRC columns showed a significant effect of the bond condition (bar texture, bar diameter, and external FRP confinement) between FRP bars and concrete on the performance of the FSRC columns. In the following sections, a numerical bond-based study on the FSRC column is presented to clearly find out the effect of different bond parameters on the lateral response of FSRC columns and to nominate the optimum bond conditions between FRP bars and concrete to ensure the damage-controllable structure.

3.2. Modeling strategy

A 3D-FE column model was created using ANSYS code version 13 [33] based on the previously given details for concrete geometry and reinforcements; see Fig. 4. In the proposed FE model, element types, material models, bond-slip laws, and boundary conditions were carefully nominated and employed to simulate the performance of both SRC and FSRC columns. Details of the FE strategy are as follows:

3.2.1. Elements-description

From the element library of ANSYS code [33], four elements were selected to simulate the behavior of the column specimens. 3D 8-node solid structural element (SOLID65) was used to model the concrete of the columns. The solid element has eight nodes with three degrees of freedom at each node: translations in the nodal x , y , and z directions. This element models concrete cracking in three orthogonal directions and concrete crushing and treats the nonlinear behavior of concrete (plastic deformation). Concrete of column footing was modeled using a 3D 8-node structural element (SOLID185) defined by eight nodes having three degrees of freedom at each node (translations in the x , y , and z directions). In addition, this element was applied to model the rigid steel plates, which were used at loading locations (Fig. 4). Longitudinal steel bars, steel stirrups, and FRP bars were represented by 3D 2-node structural bar elements (LINK180). It is noteworthy that this element has three degree of freedom (translations in the x , y , and z directions) and has capability of plastic deformations. In the light of the study by Sato and Ko [36], the authors here adopted LINK180 elements to also model the external BFRP jackets, where each line of the link elements represents a 25 mm wide (i.e., height of concrete element) of the BFRP jacket and thus LINK180 is defined by two nodes along the element's length with three translational degrees of freedom at each edge node. To consider sensitivity of the column behavior to the effects of several bond conditions, the spring element (COMBIN39) of zero length was used to connect the nodes of the LINK180 elements of the longitudinal reinforcement to both concurrent SOLID65 and SOLID185 elements using the generalized force-deflection curves, i.e. bond-slip relationship as it will be addressed in detail in the following sections. The concurrent nodes between the LINK180 and SOLID65 and also between the LINK180 and or SOLID185 elements were coupled in both the transverse and lateral directions. However, bond between the BFRP sheet and the adjacent

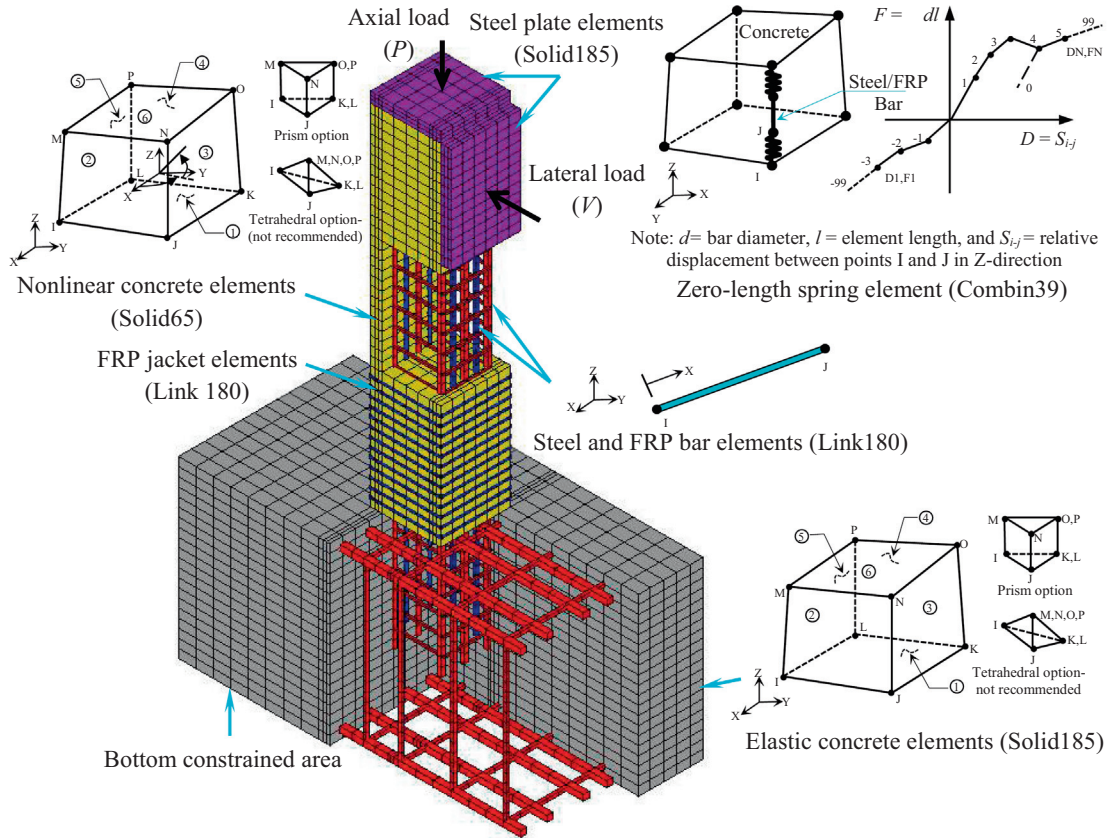


Fig. 4. Typical 3D FE model of simulated FSRC column specimens.

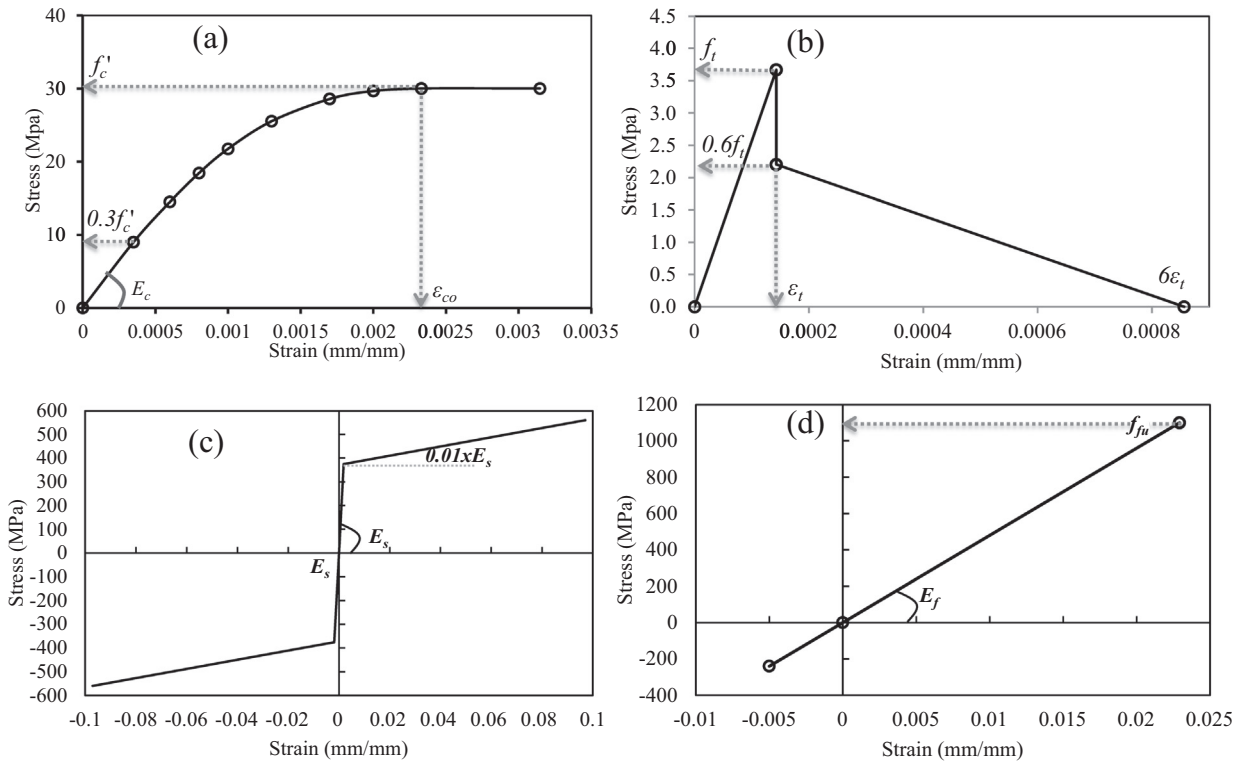


Fig. 5. (a) Stress–strain model of concrete in compression [38], (b) Stress–strain model of concrete in tension [39], (c) Bilinear stress–strain model for reinforcing steel [41], and (d) Elastic stress–strain model of FRP bars.

concrete surfaces was assumed perfect (i.e., the nodes of the elements representing the BFRP sheets and that of concrete elements were coincided).

3.2.2. Material models

Cracking of the concrete in the tensile zones, nonlinearity of the concrete in compression, and plasticity of the steel reinforcement were taken into account to simulate the causes for nonlinearity. To simulate the material properties of the Solid65 elements, the procedure used in the work of Wolanski [37] on RC flexural beam was adopted. The nonlinear plastic behavior of concrete in compression was defined using the MacGregor model [38], Fig. 5a, while the concrete tensile stress–strain response was modeled using the ACI model [39], Fig. 5b. In both models, f'_c is the maximum concrete compressive strength and ε_{co} is the corresponding axial strain = $2 f'_c/E_c$, f_t is the ultimate tensile strength = $0.62 (f'_c)^{0.5}$, and E_c is the modulus of elasticity of concrete. The concrete Poisson's ratio was assumed equal to 0.2. The open and closed shear coefficients, which are typically in the range of zero to 1.0, were taken as 0.3 and 0.9, respectively. Additionally, the constitutive concrete model by William and Warnke [40] was used to define when failure will occur in concrete elements. It worth mentioned that the concrete of the column base was simulated with elastic concrete material properties having the same modulus of elasticity and Poisson's ratio of the concrete of the column.

The nonlinear response of the steel reinforcing bars was assumed to be bilinear elasto-plastic with a strain–hardening ratio of 0.01 [41]; see Fig. 5c. Steel Poisson's ratio was specified as 0.3. The FRP longitudinal reinforcement and FRP jacketing were modeled as a simplified uniaxial elastic material with similar modulus of elasticity in tension and compression, Fig. 5d. Finally, the rigid steel plates of loading were simulated with elastic steel material properties having a modulus of elasticity and Poisson's ratio of 200 GPa and 0.3, respectively.

3.2.3. Bond–slip modeling

As the results of the experimental investigations showed a significant effect of the bond condition between reinforcing bars and concrete, it was very necessary to include the bond–slip models in the FE models to accurately simulate the performance of the tested specimens. Therefore, the following bond–slip relations for the FRP and steel bars were adopted.

3.2.3.1. FRP bond–slip model. In the present FE modeling, different bond conditions for FRP-to-concrete were considered. For the FSRC columns those reinforced with 10-mm-diameter BFRP bars, two bond conditions were considered for each column: perfect bond was assumed in the first one while the bond–slip models of the bars B10-S and B10-DH10 (see Table 1 and Fig. 1b) were adopted in the second one to simulate the FRP bond behavior in the columns CSF-2.8%-IS-D10-J and CSF-2.8%-IR-D10-J, respectively. For the FSRC column that reinforced with 6-mm-diameter BFRP bars (CSF-2.8%-ES-D6-J), the experimental results indicated different bond conditions for the corner and intermediate FRP bars. Therefore, special treatment for bond conditions between FRP bars and concrete was performed, as will explained in a following section.

3.2.3.2. Steel bond–slip model. CEB-Code model [42] was adopted in this study to model the bond–slip behavior between longitudinal steel bars and concrete. This model consists of the same three parts of the BPE model that was described earlier and shown schematically in Fig. 1a. The parameters of this model have been prescribed for confined and unconfined normal strength concrete with good or other bond conditions [42]. In this study, ribbed steel bars were used and good confinement from stirrups and FRP jacketing (if

any) was expected. Therefore, good bond conditions between steel bars and concrete were assumed, thereby parameters of the bond–slip model of steel-to-concrete were kept constant in all cases studied meanwhile different bond conditions for FRP-to-concrete were examined. For the case of good bond condition, the parameters of steel bond–slip law were defined as follows: $\tau_1 = 2.5(f'_c)^{0.5}$; $\tau_2 = 0.4\tau_1$; $S_1 = 1$ mm; $S_2 = 3$ mm; $S_3 =$ distance between ribs = 10.5 mm; and $\alpha = 0.4$. To assess the effect of steel bond–slip on column behavior under the effect of lateral loading, lateral response of SRC column was examined when bond between steel bars and concrete is perfect.

3.2.4. Loading and nonlinear solution

The first load step of all column models was applying an axial compressive load of 40 kN at the top end of the column models. After that a stepwise increasing process of a monotonic lateral load at 850 mm above the column base was applied. It is noteworthy that during the experimental study of Ibrahim et al. [32] the applied axial load increased linearly with the increase in lateral deformation to record 80 kN at the ultimate drift capacity and thus a stepwise increasing process of the applied axial load was also considered in the numerical simulation. An automatic time stepping was adopted to predict and control load step sizes. At the end of each load step, convergence was checked using Newton–Raphson equilibrium iterations to satisfy a predefined tolerance limit of the convergence criteria. The convergence criteria were based on equilibrium of forces and compatibility of displacement. Due to the complex nature of the models, convergence was difficult to be achieved by the default value of ANSYS. Therefore, the convergence tolerance limit was increased to give a displacement convergence criterion of 0.25 during the nonlinear solution [37].

3.2.5. Failure criteria

For the SRC column, since there is no direct capability to simulate the buckling of steel bars in ANSYS, solution was stopped once the lateral displacement reached a limit comparable to the maximum achieved displacement recorded during the experimental test before failure. For the FSRC columns, solution was stopped once the lateral load reduced suddenly or gradually to a value comparable to the lateral strength of the SRC column.

3.3. Verification of the finite element models

This section compares the results of numerical simulation with those experimentally defined for the four column specimens (CS-2%, CSF-2.8%-IS-D10-J, CSF-2.8%-IR-D10-J, and CSF-2.8%-ES-D6-J). This comparison could provide some evidences about applicability of the created model to adequately simulate the structural performance of bond-controlled FSRC columns. Fig. 6 compares the load–displacement relationships from the FE analyses with the experimental average skeleton curves of push and pull loading directions of the four specimens. For comparison, different response characteristic points of the load–displacement relationships were studied: yield load V_y and ultimate load V_u and the corresponding lateral displacements δ_y and δ_u , respectively, as well as peak load V_p which was characterized by two lateral displacements δ_{p1} and δ_{p2} . Definitions of these points can be seen in the idealized structural performance shown in Fig. 8a. Table 4 includes the corresponding values from both the experimental and numerical analyses. Moreover, Fig. 7 shows a comparison between the measured axial strains in FRP bars and the corresponding values defined numerically in a relationship with the applied lateral load. The following subsections would provide a detailed comparison between numerical and experimental results.

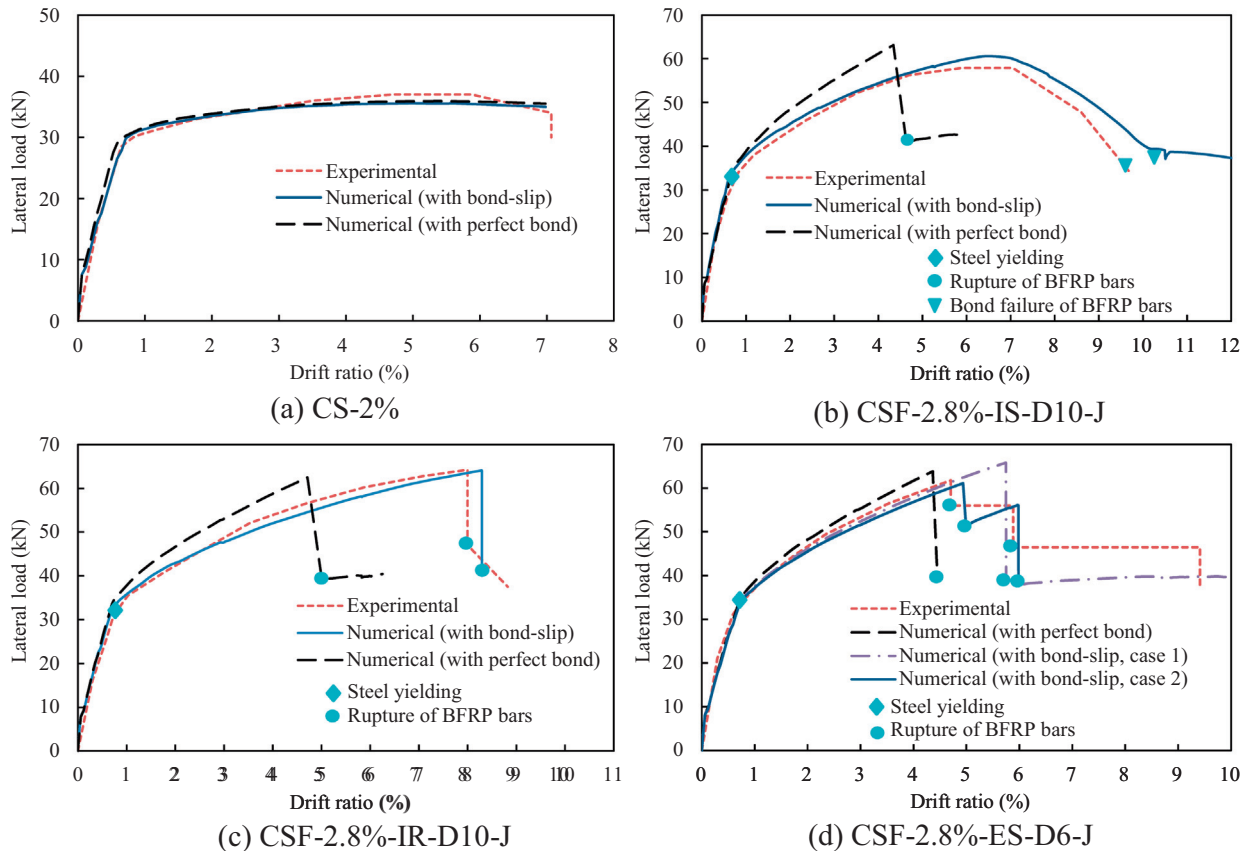


Fig. 6. Numerical and experimental load-drift ratio relations of the tested columns.

3.3.1. SRC column (CS-2%)

For the column CS-2%, Fig. 6a shows that the load–displacement plot from the FE analysis agrees well with the experimental data. This figure also shows that there is a slight effect from steel bond behavior on the lateral performance of the SRC column. For instance, the yielding load and its corresponding displacement were approximately the same as those of the experimental results; see Table 4. After yielding, the experimental column showed somewhat greater stiffening than that defined numerically for both cases with or without bond effect. It must be noted that in ANSYS FE modeling there is no direct capability of simulating buckling of steel reinforcement, and thus both the failure mode and the ultimate displacement could not be predicted and the numerical simulation was terminated at lateral displacement equal to that experimentally achieved.

3.3.2. FSRC columns: CSF-2.8%-IS-D10-J and CSF-2.8%-IR-D10-J

Fig. 6(b) and (c) show a comparison between the average skeleton curve of each of CSF-2.8%-IS-D10-J and CSF-2.8%-IR-D10-J columns experimentally tested, respectively, and the numerical results for two different bond conditions, e.g. the first case is perfect bond between BFRP bars and concrete and the latter case reflects the effect of bond properties defined in Table 1 for both smooth BFRP bars (B10-S) and roughened BFRP bars (B10-DH10). It is evident from these figures that overlooking the effect of bond condition between BFRP bars and concrete (assuming perfect bond between FRP bars and concrete) overestimates the inelastic lateral resistance of the FSRC columns and thus column ductility would be underestimated due to early rupture of BFRP bars. However, FE results of both columns have a good correlation with the experimentally defined responses when bond effect of BFRP bars to the

surrounding concrete was included in the numerical simulation. For instance, beyond the yielding load, the trends of the experimental and numerical curves of the column CSF-2.8%-IS-D10-J (with smooth BFRP bars) were identical and consisted of hardening zone up to the peak lateral strength, then a stability zone over which the peak strength is maintained before entering the degradation zone. It should be noticed that the model, however, overestimates displacement at the descending branch during failure, e.g. 18% higher than the counterparts experimentally measured. This overestimation is most probably due to the effect of other factors rather than the bond–slip between the FRP bars and concrete such as buckling of steel bars. In addition, the entire load–displacement response of the FE model of column CSF-2.8%-IR-D10-J (with roughened FRP bars) compares very well with the experimental response. And failure modes of both numerical and experimental tests were due to sudden rupture of BFRP bars.

In order to confirm the importance of including bond conditions of BFRP bars, Fig. 7(a) and (b) show the experimentally recorded axial strains of BFRP bars versus column lateral drifts, and the counterpart FE results for different bond conditions of BFRP bars are superimposed on the same figures for comparison. These figures show that, up to yielding of steel bars, there is no clear effect for bond conditions on the strain values induced in FRP bars as both experimental and numerical results are almost coincident. However, with further displacing the columns, a significant difference could be realized for bond conditions on strain values in FRP bars. For perfect bond condition between FRP bars and concrete, axial strains in FRP bars from the FE models at all drift levels were much higher than those recorded during the experimental tests. On the other hand, when bond–slip between the FRP bars and concrete was considered, the lateral drift–strain plots obtained from

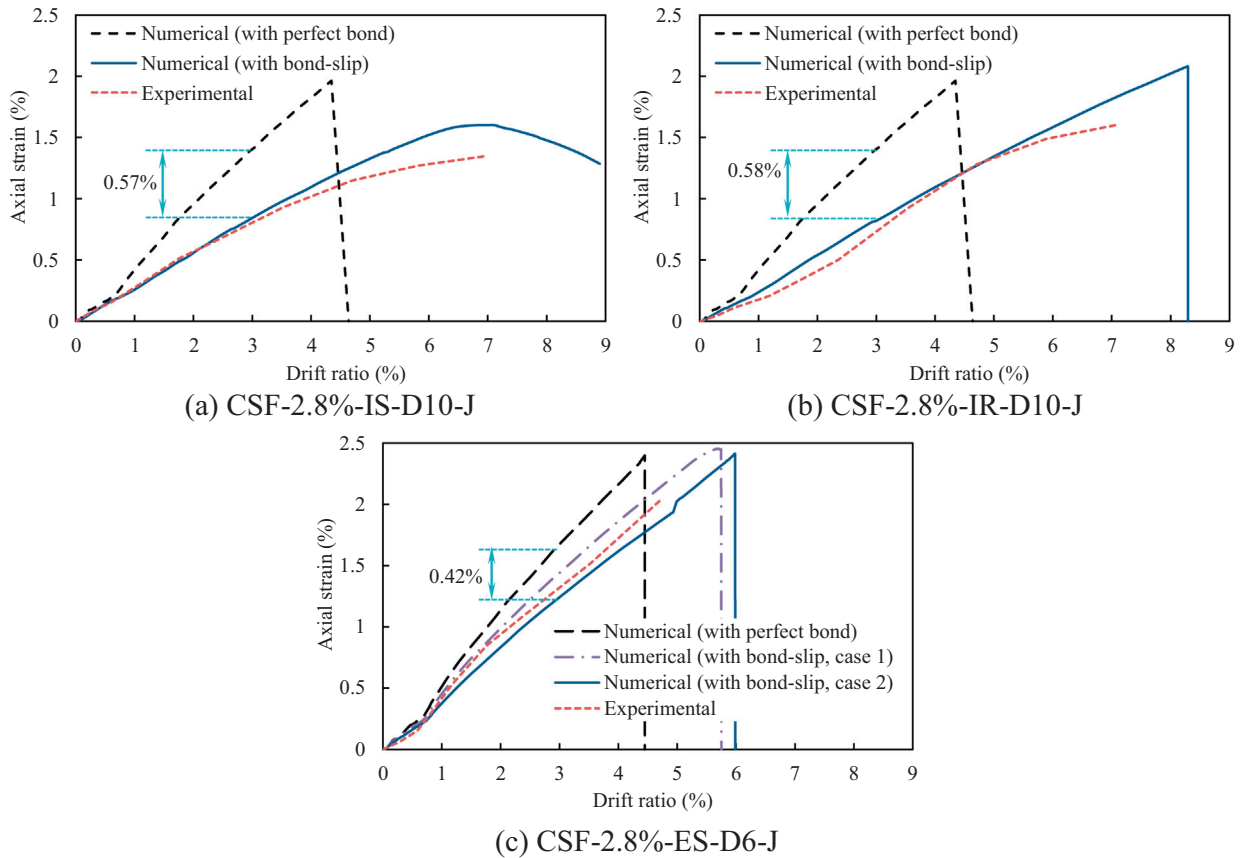


Fig. 7. Numerical and experimental drift ratio-FRP strain relations of the tested columns.

the FE models correlated very well with the experimental results up to the drift levels where no further readings from the strain gauges could be recorded: during experimental work unfortunately not all strain gauges were able to record induced values up to the ultimate drifts. It should be noticed that, the measured strains were less than the predicted values at high drift levels over 5%. For instance, the predicted strains of FRP bars in the two columns CSF-2.8%-IS-D10-J and CSF-2.8%-IR-D10-J at lateral drift of 7% were approximately 18% and 14% more than the measured strains, respectively. The differences between the experimental and numerical strains is possibly due to one or more reasons as follows: (1) the cyclic loading procedure during the experimental tests causes local buckling to the BFRP bars and hence slightly mitigate their contribution to resist the lateral loads while there is no such buckling simulation in the created FE model; (2) for each pair of BFRP bars placed on the two opposite sides of the models, the strains are uniformly distributed while they would not be uniform in the experimental columns; and (3) it would be possible that placement of BFRP bars in the test models was not exactly similar to their right places.

3.3.3. FSRC column: CSF-2.8%-ES-D6-J

In the light of the experimental results of CSF-2.8%-ES-D6-J column, bond behavior of BFRP bars placed close to column corners was different from that of the middle BFRP bars. This observation would require special concern during FE simulation of such different bond behaviors. So, first, bond between all FRP bars and concrete was assumed perfect. In another simulation, which is named here case 1, a bond-slip model was adopted between all BFRP bars and concrete, in which bond strength τ_1 and the

corresponding slip S_1 were 20 MPa and 1.1 mm, respectively. The value to τ_1 was defined based on the applied pull out force on B10-S and S_1 is the corresponding slip value; see Table 1. In another trial to mimic the experimental observations for the different bond behavior of BFRP bars, another model named (case 2) considered two different bond-slip conditions for the corner and intermediate bars, where τ_1 and S_1 were 20 MPa and 0.25 mm for the corner bars, respectively and τ_1 and S_1 were 20 MPa and 5 mm, for the intermediate bars, respectively. Here, the authors defined the values of S_1 of each bond-slip model based on large number of iterative numerical trials for both the corner and intermediate bars until the numerical and experimental results correlate well with each other in terms of load-drift ratio and drift ratio-strain relations. From Fig. 6d and Table 4, up to the steel yielding, all numerical cases shared approximately the same elastic zone with the experimental result. Beyond the yielding of steel bars, when perfect bond was assumed between BFRP bars and the surrounding concrete, rupture of all BFRP bars of the numerical model was occurred at approximately the same drift level corresponding to rupture of the corner BFRP bars during the experimental loading of this column. In case a unified bond-slip model was assumed for all FRP bars, the column would be able to show gradual increase in lateral strength to a drift ratio higher than that defined experimentally. It was interesting to find that rupture of all BFRP bars of the numerical model (case 1) approximately occurred at a drift level corresponding to the onset of experimental rupture of the intermediate BFRP bars. However, in the numerical model (case 2), ruptures of the BFRP bars were first for the corner BFRP bars at drift levels of 4.9% and then it occurred for the intermediate bars at 6% lateral drift.

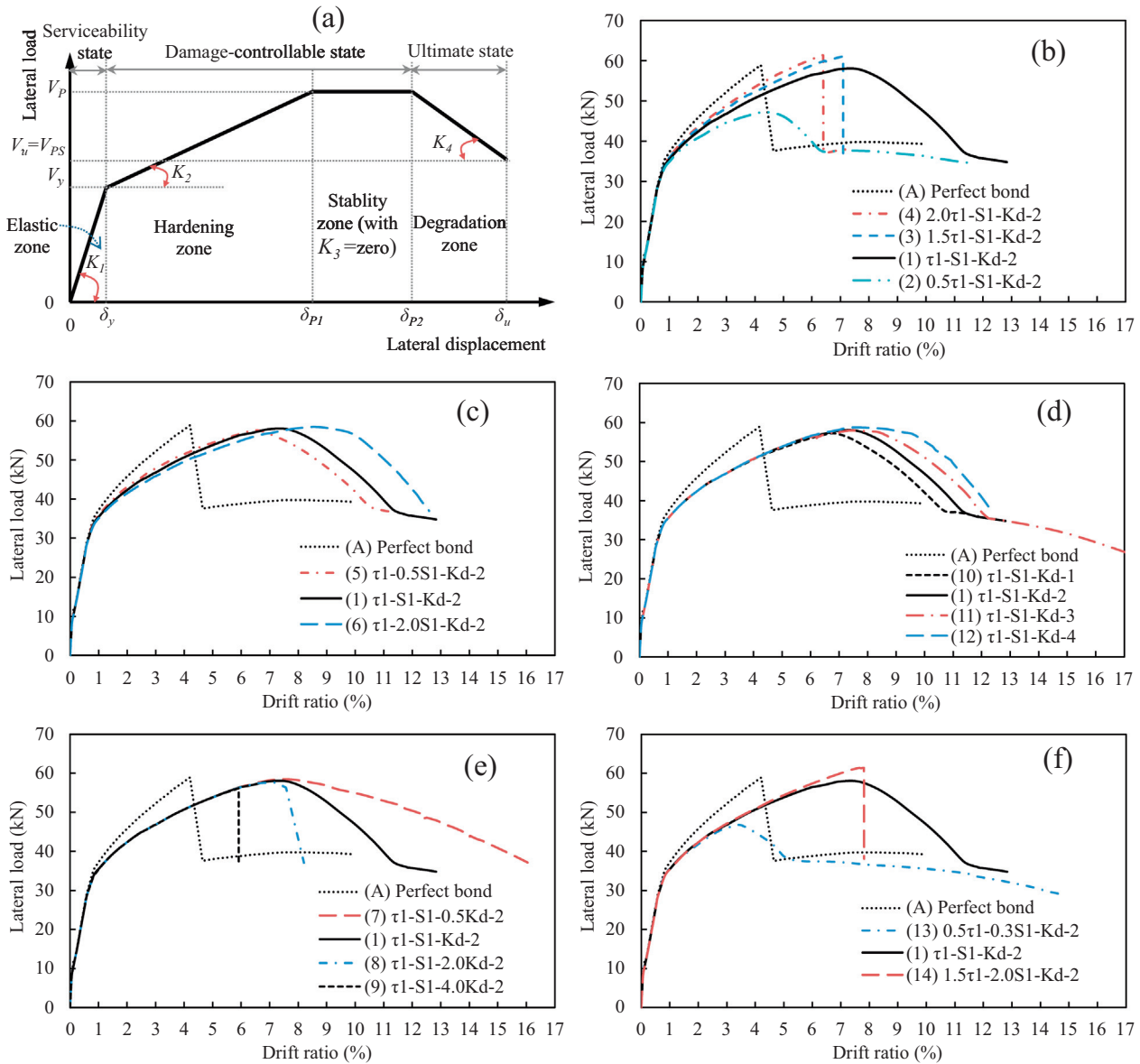


Fig. 8. (a) Idealized load–deformation relation of FSRC columns, and (b)–(f) effect of bond–slip parameters on the load–deformation of the FSRC column.

Table 4
Load–deformation characteristic values of the tested columns.

Specimen	Test type	V_y (kN)	δ_y (mm)	V_p (kN)	δ_{p1} (mm)	δ_{p2} (mm)	V_u (kN)	δ_u (mm)	Failure mode
CS-2%	Experimental	27	5.7	38	30	50	30	59	Buckling
	Numerical (with bond slip)	28	5.8	35	32	59	N/A	N/A	N/A
CSF-2.8%-IS-D10-J	Experimental	32	7.4	57	47	59	38	73	Bond
	Numerical (with bond slip)	34	6.3	60	50	61	39	86	Bond
CSF-2.8%-IR-D10-J	Experimental	29	6.2	65	70	70	38	70	Rupture
	Numerical (with bond slip)	32	6.0	64	71	71	35	71	Rupture
CSF-2.8%-ES-D6-J	Experimental	33	6.4	62	40	40	38	80	Rupture
	Numerical (with perfect bond)	35	6.2	64	37	37	35	37	Rupture
	Numerical (with bond slip, case 1)	35	6.2	65	48	48	35	48	Rupture
	Numerical (with bond slip, case 2)	35	6.2	61	42	42	35	52	Rupture

Fig. 7c shows the drift ratio–axial strain relations of both the numerical models with bond–slip considerations and the experimental results, and it is recognizable that the measured strain values have a good agreement with those defined from the numerical model of case 2. Similar to the previous finding that perfect bond

conditions between FRP bars and concrete overestimate the strain values and thus early termination is expectable in this case; Fig. 7c. Nevertheless, close-up examination for the difference between strain values in FRP bars when bond–slip is considered or overlooked for both CSF-2.8%-ES-D6-J and CSF-2.8%-IS-D10-J columns,

this difference is 0.42% for CSF-2.8%-ES-D6-J column and is 0.57% for CSF-2.8%-IS-D10-J column. From the authors' point of view, this would be an indication about the good bond performance of small diameter FRP bars than larger diameter FRP bars.

In conclusion, the results of the adopted FE models compared well with the structural responses of both the SRC and FSRC columns. Consequently, the developed 3D FE model could examine sensitivity of the lateral response of FSRC columns to several bond conditions between FRP bar and concrete in an attempt to define the optimum bond design parameters ensuring the required performance, as presented in the following sections.

4. Numerical bond-based parametric study on the FSRC columns

Although experimental studies would be helpful to realize the effect of different bond parameters on the performance of FSRC columns, a comprehensive systematic program would be required to appropriately define the effect of several bond parameters on the characteristic stages of damage-controllable structures: elastic stage (serviceability stage), post-yield stage (damage-controlled stage), and ultimate stage. The FE model created in this study has demonstrated that it is possible to examine sensitivity of structural performance of FSRC columns to bond behavior of FRP bars in concrete. Therefore, this section presents the numerical results of a parametric study carried out using the developed FE model to investigate the effects of altering the parameters of FRP bond-slip model on the structural performance of FSRC columns. Initial values for the parameters of the bond-slip model of FRP bars were required to represent a reference bond-slip condition. So, bond-slip model of the smooth BFRP bar (B10-S) of the FSRC CSF-2.8%-IS-D10-J column (Fig. 1b and Table 1) was considered as a reference condition.

4.1. Proposed numerical investigations

The 3-D FE model created using ANSYS (Fig. 4) was applied to study the effects of several bond conditions of BFRP bars through 14 cases in addition to the perfect bond condition, see Table 5: Case A represents perfect bond condition, case 1 represents the reference case, and 13 cases show the effect of bond-slip of FRP bars parameters on column behavior. In all cases, details of the longitudinal and transverse steel and FRP reinforcements are the same and mechanical characteristics of all materials used are kept constant, so the only parameter that would affect the column lateral response

to the applied load is the bond-slip behavior of FRP bars. Generally, when FRP type and bar diameter are the same, bond behavior of FRP bars could be controlled based on the surface condition such as smooth surface bars, sand coated bars, sand blasted bars, and bars with different-detailed ribs (one directional ribs or x-ribbed surface). For example, through the aforementioned bond investigations on BFRP bars, it was found that values for τ_1 was 7.2 MPa for smooth bars and increased by 174% due to roughening bar surface; value for S_1 increased from 0.9 mm to almost double (1.7 mm) when spacing between bar ribs increased from 5 mm to 10 mm; and the value of K_d could be reduced from 1.2 to 0.6 when surface indentation changed from deeply ribbed to small indentation (almost smooth surface). Additionally, geometry dimension of ribs (height and spacing) of FRP bars would greatly affect the bond-slip behavior. In this numerical test, sensible ranges for the characteristic parameters of the bond-slip relationship were studied to examine the probability of controlling the lateral response of FSRC column in order to achieve the aim of the ductile-recoverable performance. Using the BPE Model [35], 13 bond-slip cases were studied as follows: (1) three cases reflecting the impacts of different values of the bond strength starting from 3.6 MPa to 14.4 MPa; (2) two cases presenting the effect of the definition of the FRP bar slip at the maximum attained bond strength; (3) three cases examined the influence of fracture energy of the bond-slip relationship (effect of k_d); and (4) three cases showed the effect of the existence of plateau zone at the maximum bond strength, and so S_2/S_1 ratios of 1, 3, and 4 were studied. Eventually, combined effect of both τ_1 and S_1 were studied in the last two cases. It is worth to mention here that, since no significant difference in the values of α and τ_2/τ_1 were observed in the bond investigations (Table 1), their effects were not included in the present study.

4.2. Results of parametric study and discussion

4.2.1. Required ductile-recoverable performance of FSRC columns

Fig. 8a presents the idealized load-deformation behavior (i.e., $V-\delta$ curve, where V and δ are the lateral load and lateral displacement, respectively) for the required ductile-recoverable performance of FSRC systems. More details about the mechanical model proposed for the FRP-RC damage-controllable modern bridges can be found in in the study of the authors [32]. Shortly, in this model, the structural performance consisted of four zones as follows: (1) elastic zone which ends by yielding of steel bars (V_y and δ_y), with initial elastic stiffness, K_1 ; (2) hardening zone which includes post-yield stiffness, K_2 , up to the peak lateral strength (V_p and δ_{p1}); (3) stability zone of the peak strength (with

Table 5
Details of the investigated bond properties.

Case	ID	Bond-slip parameters				Remarks
		τ_1	S_1	K_d	S_2/S_1	
A	Perfect bond	Perfect bond				
1	$\tau_1 - S_1 - K_d - 2$	7.20	1.10	0.6	2	Reference parameters
2	$0.5\tau_1 - S_1 - K_d - 2$	3.60	1.10	0.6	2	Effect of bond strength (τ_1)
3	$1.5\tau_1 - S_1 - K_d - 2$	10.80	1.10	0.6	2	
4	$2.0\tau_1 - S_1 - K_d - 2$	14.40	1.10	0.6	2	
5	$\tau_1 - 0.5S_1 - K_d - 2$	7.20	0.55	0.6	2	Effect of S_1
6	$\tau_1 - 2.0S_1 - K_d - 2$	7.20	2.20	0.6	2	
7	$\tau_1 - S_1 - 0.5K_d - 2$	7.20	1.10	0.3	2	Effect of fracture energy
8	$\tau_1 - S_1 - 2.0K_d - 2$	7.20	1.10	1.2	2	
9	$\tau_1 - S_1 - 4.0K_d - 2$	7.20	1.10	2.4	2	
10	$\tau_1 - S_1 - K_d - 1$	7.20	1.10	0.6	1	Effect of plateau zone (S_2/S_1)
11	$\tau_1 - S_1 - K_d - 3$	7.20	1.10	0.6	3	
12	$\tau_1 - S_1 - K_d - 4$	7.20	1.10	0.6	4	
13	$0.5\tau_1 - 0.3S_1 - K_d - 2$	3.60	0.33	0.6	2	General cases
14	$1.5\tau_1 - 2.0S_1 - K_d - 2$	10.80	2.20	0.6	2	

Table 6
Characteristic values of load–deformation curves and failure modes of numerical column models.

Case	Column ID	V_y (kN)	δ_y (mm)	V_p (kN)	δ_{p1} (mm)	δ_{p2} (mm)	V_u (kN)	δ_u (mm)	Failure mode
A	Perfect bond	35.0	6.5	61.0	36.0	36.0	37.0	36.0	Rupture of FRP
1	$\tau_1 - S_1 - K_d - 2$	33.3	6.3	57.9	55.0	66.0	37.0	98.0	Bond–slip
2	$0.5\tau_1 - S_1 - K_d - 2$	32.9	6.2	47.1	32.0	40.0	37.0	74.0	Bond–slip
3	$1.5\tau_1 - S_1 - K_d - 2$	33.4	6.2	61.1	60.0	60.0	37.0	60.0	Rupture of FRP
4	$2.0\tau_1 - S_1 - K_d - 2$	33.6	6.2	61.5	54.0	54.0	37.0	54.0	Rupture of FRP
5	$\tau_1 - 0.5S_1 - K_d - 2$	33.7	6.2	57.6	50.0	58.0	37.0	91.0	Bond–slip
6	$\tau_1 - 2.0S_1 - K_d - 2$	32.9	6.2	58.5	64.0	78.0	37.0	110.0	Bond–slip
7	$\tau_1 - S_1 - 0.5K_d - 2$	33.3	6.2	58.5	57.0	71.0	37.0	136.0	Bond–slip
8	$\tau_1 - S_1 - 2.0K_d - 2$	33.3	6.2	57.6	53.0	62.0	37.0	65.0	Bond–slip
9	$\tau_1 - S_1 - 4.0K_d - 2$	33.3	6.2	56.1	50.0	50.0	37.0	50.0	Rapid bond failure
10	$\tau_1 - S_1 - K_d - 1$	33.3	6.2	57.2	53.0	62.0	37.0	95.0	Bond–slip
11	$\tau_1 - S_1 - K_d - 3$	33.3	6.2	58.0	59.0	72.0	37.0	101.0	Bond–slip
12	$\tau_1 - S_1 - K_d - 4$	33.4	6.2	58.7	58.0	77.0	37.0	105.0	Bond–slip
13	$0.5\tau_1 - 0.3S_1 - K_d - 2$	33.7	6.2	46.8	26.0	31.0	37.0	63.0	Bond–slip
14	$1.5\tau_1 - 2.0S_1 - K_d - 2$	33.4	6.2	61.4	66.0	66.0	37.0	66.0	Rupture of FRP

zero stiffness (K_3)), whereby structure system demonstrates a desirable ductile performance up to a displacement of δ_{p2} before degradation of strength; and (4) degradation zone with gradual degradation of strength with a stiffness K_4 , where failure of the FSRC system is defined when the contribution of FRP bars to the lateral resistance is completely lost at a point represented by $V_u = V_{ps}$ and δ_u , where V_{ps} is the peak lateral strength of the SRC system (i.e., the column CS-2% in this study). Column performance can be divided here to three main states: serviceability state ends at yielding of steel bars, damage-controllable state which includes both the hardening zone and the stability zone, and the ultimate state represents the failure zone.

With regard to the idealized load–deformation response, Table 6 summarizes the characteristic values of the load–deformation curves and the final failure modes of the fifteen cases studied numerically. Effects of the investigated bond parameters on the lateral load–deformation response of FSRC column are depicted in Fig. 8(b)–(f) for all of the studied cases. To define the end of the serviceability state, strain values in all elements representing steel bars were scrutinized to define the first yielding load and the corresponding displacement. At the peak achieved lateral strength, through close-up examination of the load–deformation response of each of the studied cases, the authors carefully examined the existence of the stability zone and hence the corresponding displacements (δ_{p1} and δ_{p2}) were identified. Ultimately, based on failure mode of each case numerically tested, the ultimate load and the corresponding displacement were defined. It should be noticed that solution of each executed model was stopped once the lateral load reduced suddenly or gradually to a value

comparable to the lateral strength of the SRC column, as seen in Fig. 8 and Table 6. To define whether BFRP bars attained the full strain capacity or not, axial strain values at column–footing interface were checked.

4.2.2. General behavior and failure modes

Fig. 8(b)–(f) show that each of the cases studied has a distinctive post-yielding response, however, the listed values of V_y and δ_y in Table 6 means that lateral load–deformation responses of all cases share the same elastic stiffness. Although perfect bond condition would not certainly be a practical case, it was interesting to investigate the effect of large bond strength between FRP bars and concrete for comparison. Fig. 8(b)–(f) indicate that perfect bond condition would cause early termination of the gradual increase in column strength after yielding. A similar response would be when bond–slip relation was considered in the numerical analysis while bond strength equals half of the reference value (case 2), Fig. 8b. Failure modes in both cases are different, where perfect bond condition would result in rupture of BFRP bars at a drift of 4.2%. On the other hand, the low drift capacity of case 2 could be attributed to slippage of FRP bars at a drift of 4.7%. At which time strain in FRP bars started to decrease, meanwhile strain in steel bars dramatically increased up to a lateral drift of 6.4%; see Fig. 9a which shows the relationship between axial strain in FRP bars and steel bars versus column lateral drift for case 2. This figure shows also that maximum strain of BFRP bar at the critical section (column–footing interface) was less than the ultimate strain capacity of BFRP bars. Case 13 ($0.5\tau_1 - 0.3S_1 - K_d - 2$) would have a similar failure mode of case 2, where slippage of FRP bars started

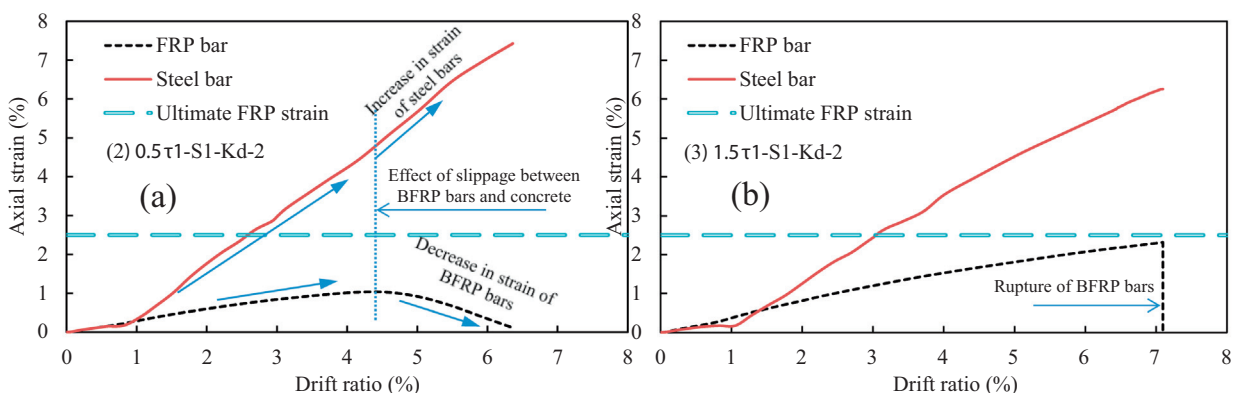


Fig. 9. Axial strain in FRP bars and steel bars at column–footing interface of the representative F-SRC columns.

earlier at a drift of 3.4%, Fig. 8f. In addition, although the column in case 9 ($\tau_1 - S_1 - 4.0K_d - 2$) could continue carrying load up to a higher lateral drift, the column at a drift of 6.4% shows a sudden drop in resisting additional lateral forces due to rapid decrease in bond strength between FRP bar and the surrounding concrete, as seen in Fig. 8e. This sudden drop is attributed to the sharp slope of the descending branch of the bond–slip relationship of FRP bars. In case 8 ($\tau_1 - S_1 - 2.0K_d - 2$), the slope K_d is half that of case 9, and so the column could achieve a later drift of 7.4% before encountering a degradation in resisting lateral loads; however, a sudden drop in column strength could be realized from Fig. 8.e. In case 3 ($1.5\tau_1 - S_1 - K_d - 2$) and case 14 ($1.5\tau_1 - 2.0S_1 - K_d - 2$), column could attain lateral drifts of 7.1% and 7.7%, respectively, and the increase in drift capacity of the FSRC columns before failure could be linked with the increase in bond strength up to $1.5\tau_1$ (case 3) or in both the bond strength and the corresponding slip (case 14). However, failure in both cases was due to rupture of FRP bars. Further increase in bond strength after this limit caused a rapid rupture of FRP bars, where case 4 ($2.0\tau_1 - S_1 - K_d - 2$) attained lateral drift of 5.5% before the rupture of FRP bars. In all other cases (1, 4, 5–7, and 10–12), they would have a ductile failure mode after achieving the peak strength due to bond degradation between FRP bars and concrete, see Table 6.

4.2.3. Initial and post-yield stiffness

In general, the bond strength of FRP bars with concrete showed no sound effect on the yielding load and the corresponding lateral displacement, and all columns shared approximately the same initial elastic stiffness, Fig. 8 and Tables 6. Before yielding of column main longitudinal reinforcement, compared to steel stiffness, FRP bars have a smaller elastic stiffness and in turn a slight contribution to column flexural deformations. In the inelastic stage, however, FSRC column showed a bond-controlled performance: slope of post-yield stiffness and column displacement at the peak strength (δ_{p1}) are highly dependent on the bond conditions. In the study of the authors Ibrahim et al. [32], the FSRC column with the previously mentioned concrete and reinforcement details was designed to attain a ductility of 10 (upper limit of moderate ductility demands [43]) and achieve a lateral strength of 66 kN (i.e., approximately twice the strength of the SRC column) through the existence of post-yield stiffness. Therefore, two indices were applied to identify the effect of altering bond parameters on column post-yield stiffness. The first index (k) was the ratio between column post-yield stiffness (K_2) and elastic stiffness (K_1), ($k = K_2/K_1\%$), and the second measure was column ductility at the end point of the achieved

post-yield stiffness (δ_{p1}/δ_y). Definitions of K_1 and K_2 were as follows:

$$K_1 = V_y/\delta_y \tag{1}$$

$$K_2 = (V_p - V_y)/(\delta_{p1} - \delta_y) \tag{2}$$

For each case of the cases numerically studied, Table 7 summarizes the values of the elastic stiffness, post-yield stiffness, column ductility at peak load, and the values of additional ductility indices that will be addressed in the following parts. Since all columns shared the same elastic stiffness, the value of k is essentially dependent on the slope of the column post-yield stiffness. Table 7 shows that the smallest value of k is 8.3% and the largest value is 16.4%. The maximum ratio was achieved when bond between FRP bars and concrete was perfect, meanwhile in all other cases value of k was almost equal to or less than 10%. Moreover, bond conditions could control column ductility corresponding to the end point of the achieved post-yield stiffness. Fig. 10 shows a relationship between each parameter of the bond–slip model and the ratio k represented on one vertical axis and the column ductility at peak strength represented on the other vertical axis. For instance, Fig. 10a shows the effect of the increase in bond strength from 3.6 MPa to infinity (perfect bond). It is noticeable that bond strengths of 3.6 to 10.8 MPa (cases 1-to-3) indicate comparable values of k , however, ductility corresponding to end point of the post-yield stiffness shifted from 5.2 to 9.7 with the increase of bond strength from 3.6 MPa (case 2) to 10.8 MPa (case 3), respectively. In case 3, the column could reach a lateral strength of 61.1 kN, however, this strength was less than the design strength (66 kN), and the corresponding column ductility was a little bit smaller than 10. In case 6, the increase in slippage of FRP bar at the maximum bond strength to double value of its counterpart of the reference case could result in a decrease in the value of k from 9.6% to 8.3%, however the ductility at the end point of post yield stiffness increased from 8.7 to 10.3. It seems that column ductility corresponding to the peak strength in case 6 is over the demand ductility, and its peak strength is 58.5 kN which is almost 89% of the design strength. Table 7 and Fig. 10c show that the ductility at the end point of the achieved post-yield stiffness is slightly affected by the increase in the slope of the descending branch of the bond–slip model (K_d), this could be observed from the reference case 1 and cases 7-to-9. In these cases, neither the ductility demand nor the design peak strength could be achieved. Compared to cases 1 and 10, FSRC columns in cases 11 and 12 show an increase in the column ductility at the peak strength when S_2/S_1 of the horizontal plateau region of the bond–slip

Table 7
Indices measuring effect of bond on column post-yield stiffness and ductility.

Case	Column ID	Initial elastic stiffness	Post-yield stiffness indices		Ductility indices		
		K_1 (kN/mm)	$k = K_2/K_1$ (%)	$\mu_{p1} = \delta_{p1}/\delta_y$	$(\delta_{p2} - \delta_{p1})/\delta_y$ (mm/mm)	μ_f (mm/mm)	$\Delta\mu = \mu_f - \mu_{p2}$
A	Perfect bond	5.4	16.4	5.5	0.0	5.5	0.0
1	$\tau_1 - S_1 - K_d - 2$	5.3	9.6	8.7	1.7	15.6	5.1
2	$0.5\tau_1 - S_1 - K_d - 2$	5.3	10.4	5.2	1.3	11.9	5.5
3	$1.5\tau_1 - S_1 - K_d - 2$	5.4	9.6	9.7	0.0	9.7	0.0
4	$2.0\tau_1 - S_1 - K_d - 2$	5.4	10.8	8.7	0.0	8.7	0.0
5	$\tau_1 - 0.5S_1 - K_d - 2$	5.4	10.0	8.1	1.3	14.7	5.3
6	$\tau_1 - 2.0S_1 - K_d - 2$	5.3	8.3	10.3	2.3	17.7	5.2
7	$\tau_1 - S_1 - 0.5K_d - 2$	5.4	9.2	9.2	2.3	21.9	10.5
8	$\tau_1 - S_1 - 2.0K_d - 2$	5.4	9.7	8.5	1.5	10.5	0.5
9	$\tau_1 - S_1 - 4.0K_d - 2$	5.4	9.7	8.1	0.0	8.1	0.0
10	$\tau_1 - S_1 - K_d - 1$	5.4	9.5	8.5	1.5	15.3	5.3
11	$\tau_1 - S_1 - K_d - 3$	5.4	8.7	9.5	2.1	16.3	4.7
12	$\tau_1 - S_1 - K_d - 4$	5.4	9.1	9.4	3.1	16.9	4.5
13	$0.5\tau_1 - 0.3S_1 - K_d - 2$	5.4	12.2	4.2	0.8	10.2	5.2
14	$1.5\tau_1 - 2.0S_1 - K_d - 2$	5.4	8.7	10.6	0.0	10.6	0.0

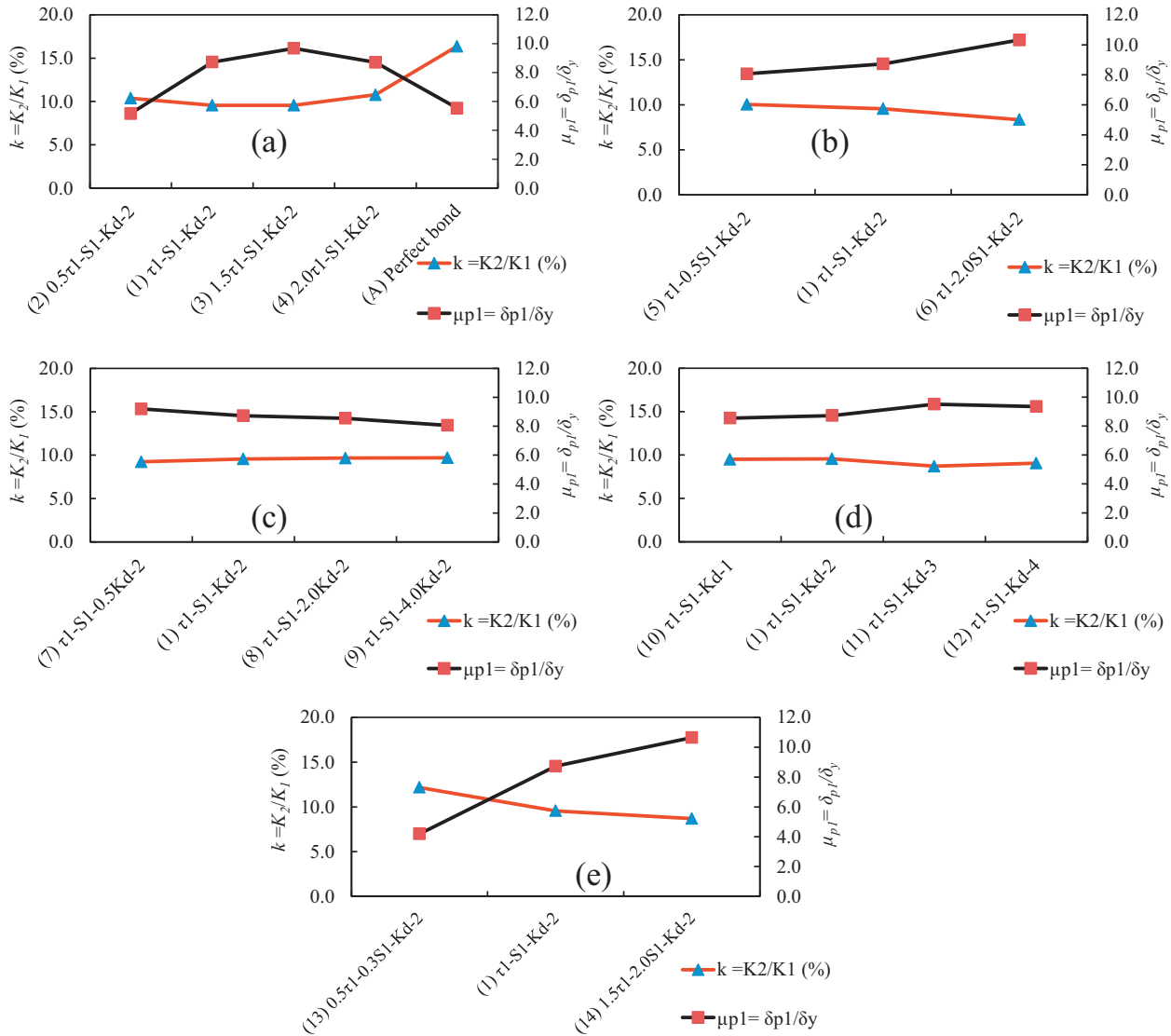


Fig. 10. Effect of studied bond-slip parameters on post-yield stiffness ratio and column ductility at the peak strength.

model is over than 2, but this factor has no clear impact on the column post-yield-stiffness ratio; as seen in Table 7 and Fig. 10d. Ultimately, two cases could successfully achieve the ductility demand of 10 at peak strength comparable with the design lateral strength, namely cases 6 and 14; see Fig. 10.

4.2.4. Ductility indices

One major concern in the damage-controlled structural system is to withstand strong earthquake with enough ductility after reaching the maximum strength, and at the end of this state the structure goes into the failure state through a gradual degradation of strength. In order to study the effect of bond-slip parameters on the required ductility afterward the achieved lateral strength, two indices were proposed and investigated as follows:

$$l = (\delta_{p2} - \delta_{p1}) / \delta_y = \text{increase in ductility in the stability zone} \quad (3)$$

$$\mu_f = \delta_u / \delta_y = \text{displacement ductility at failure point} \quad (4)$$

Eq. (3) determines the increase in ductility beyond the peak strength, and Eq. (4) defines the ultimate ductility at the failure point. Based on the proposed mechanical model of damage-controlled structural system [32], failure point should meet a required lateral

strength not less than 37 kN, which was the lateral strength of the SRC column (CS-2%). Ultimately, the gradual decreasing in column strength in the failure state was evaluated based on the increase in ductility beyond the stability zone ($\Delta\mu$), which was defined as the difference between column ductility at the failure point and column ductility at the end of the stability zone (Eq. (5)), Fig. 8a.

$$\Delta\mu = (\delta_{p2} - \delta_{p1}) / \delta_y = \text{increase in ductility in the ultimate state} \quad (5)$$

In addition to the summarized values in Table 7, Fig. 11 shows the effect of the bond-slip parameters of FRP bars on both ductility indices l and $\Delta\mu$. Fig. 11d indicates the positive effect of the existence of the plateau region of the bond-slip model of FRP bars on column ductility in the third zone of the damage-controlled structure: the increase in the ratio S_2/S_1 is accompanied with a considerable increase in the length of the stability zone. However, there is no clear effect of this bond parameter on the value of $\Delta\mu$. That is the increase in the size of the plateau region could enhance column ductility in the damage-controllable state in particular and column ductility in general. Fig. 11b shows that the increase in slip of FRP bar at the maximum bond strength could also improve column ductility in the stability zone, nevertheless

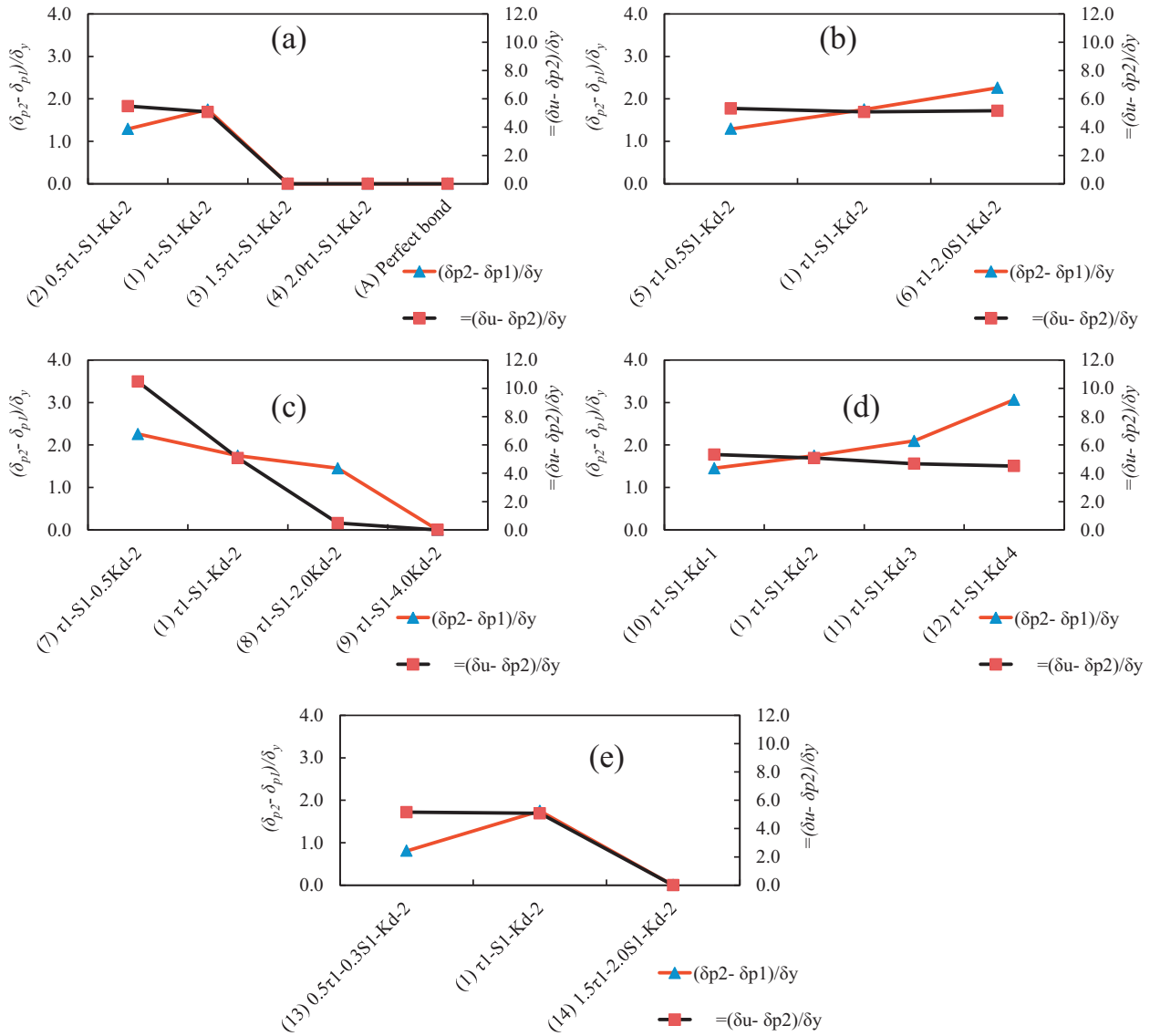


Fig. 11. Effect of studied bond-slip parameters on ductility indices in the ultimate state of FSRC columns.

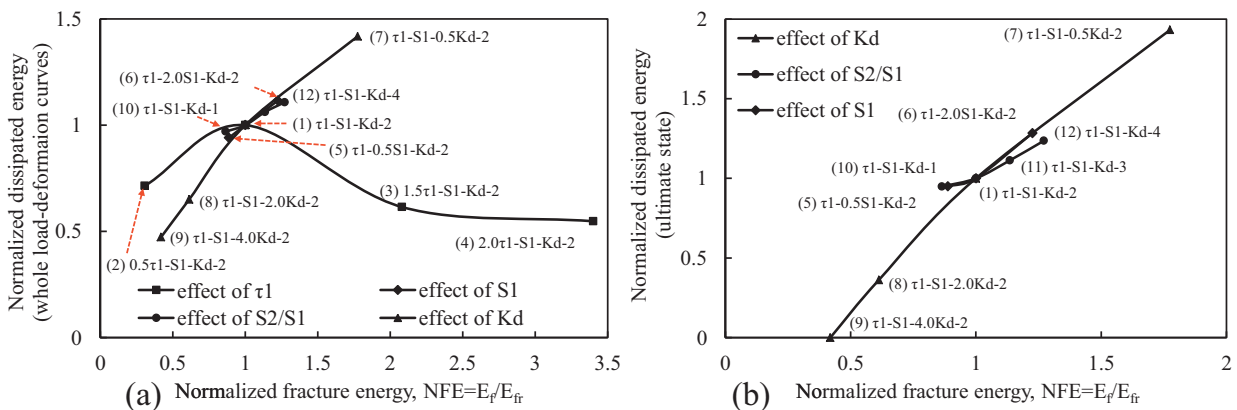


Fig. 12. Effect of FRP bond-slip parameters on dissipated energy.

it can not cause any considerable increase in the value of $\Delta\mu$. Increase in both FRP bars bond strength and the slope of the descending branch of bond-slip model adversely affect the column

ductility in the third and fourth zones in the damage-controlled FSRC column; as seen in Fig. 11(a) and (c). For instance, the increase in bond strength over 7.2 MPa could completely work

against column deformability to come into the stability zone. A similar result could be noticed for the effect of K_d when its value over 0.6 MPa/mm. With regard to ductility demand of 10 at the peak column strength, zone three of the damage-controllable structure could be realized only in case 6, Table 7. It was interesting to observe that column ductility at the end of the damage-controllable state in the cases 6, 7, 11, and 12 could be 12.6, 11.5, 11.6, and 12.5, respectively. In addition, the column ductility at failure of all these cases was over 16. In conclusion, controlled slippage between FRP bars and concrete would enhance column ductility before reaching the peak lateral strength and ensure enough ductility after the peak strength and at failure state. In other words, parameters of the bond-slip model (bond strength and its corresponding slip, the length of the plateau region, and the slope of the descending branch) can control the definition of both column deformability and lateral strength in each state of the damage-controllable FSRC structure after yielding.

4.2.5. Energy dissipation

In addition to the stiffness and ductility indices, energy dissipation of the proposed FSRC structure during major earthquakes should be carefully addressed. Fig. 12 shows the effect of investigated bond parameters on the normalized dissipated energy (NDE) versus the normalized fracture energy (NFE) of the bond-slip curves. In this figure, the fracture energy was calculated as the area enclosed by the bond-slip curves, while the dissipated energy was calculated as the area under the lateral load-displacement curves. Furthermore, the NDE and the NFE are defined as the dissipated energy and fracture energy of the case under consideration normalized by those of the reference case (case 1), respectively. To understand the effect of bond-slip properties on the dissipated energy, the NDE was calculated for the whole area of the load-displacement curves, as shown in Fig. 12a, and for only the ultimate state, as shown in Fig. 12b. As shown in Fig. 12, bond-slip parameters of FRP bars has a potential effect on the dissipated energy. Apparently from this figure, the decrease in the slope of the descending branch of the bond-slip model of FRP bars (K_d) has a favorable effect on the whole dissipated energy. By decreasing the slope of the descending branch from $4.0 K_d$ (case 9) to $0.5 K_d$ (case 7), the value of NFE increased from 0.42 to 1.78 which is accompanied with an increase in the NDE from 0.47 to 1.42, as seen in Fig. 12a. It should be noticed from Fig. 12b that this parameter has a significant effect on the dissipated energy in the ultimate state, as the increase in the bond-slip fracture energy due to gradual degradation of bond strength is accompanied by a considerable increase in the column dissipated energy during the failure time; as shown in Fig. 8e. Compared to the effect of K_d , the increase in the fracture energy of the bond-slip models by increasing the length of the horizontal plateau zone (S_2/S_1) showed much less impact on the dissipated energy. That is, increasing S_2/S_1 from 1 to 4 could only just achieve 15% increase in the NDE. As the column model with bond strength of FRP bars of $1.5\tau_1$ (case 3) suddenly failed due to rupture of FRP bars and the column model with $0.5\tau_1$ (case 2) failed due to the slippage of FRP bars at drift levels much less than that of the reference model, the dissipated energy of the two models was approximately 65% of that of the reference model (case 1), as shown in Fig. 12a.

4.3. Contribution of longitudinal steel and FRP reinforcement to deformability of FSRC column (components of lateral deformation)

To clearly understand the effect of bond parameters on ductility of the studied cases, Fig. 13 shows the strain distribution of steel and FRP bars through column height at column drift of 4.2%. This level was decided for comparison as it was the ultimate drift capacity of the case A (perfect bond). Also, column lateral load versus rotation at the column-footing interface was plotted in Fig. 14. There is a

general consensus that ductility in conventionally reinforced columns is dependent on the deformability of steel bars in the plastic hinge zone; this could be checked also from Fig. 13a. In this figure, the numerical result of the column CS-2% showed concentration of steel strains in 200 mm above the column base. On the other hand, the adopted reinforcement details using both steel and FRP bars showed a different behavior when bond was assumed perfect between FRP bars and concrete (case A): that is, after yielding of steel bars, higher propagation for steel strains could be noticed up to 400 mm from the column base, Fig. 13a. In addition, the ratio of steel strains to yield strain up to 100 mm above the column base in the FSRC column (case A) would reduce to approximately 50% of the counterpart values of the SRC column; see Fig. 13a. This distribution could be attributed to the contribution of FRP bars to the column strength which resulted in relaxation in tension forces in steel bars, and this propagation of steel deformation would compensate the reduction in the induced steel strains at column base to achieve a comparable deformation to SRC column. However, in this case (case A); the column could not attain the same ductility of the SRC column due to rupture of BFRP bars. Compared with the conventional column, when bond conditions ensure the perfect bond between the FRP bars and concrete, this would result in a mitigation of damage at the column base, however, final deformability could be smaller.

When bond-slip between FRP bars and the surrounding concrete was considered in the other cases, considerable changes in the distribution of the axial strains for both steel and FRP bars through column height could be noticed from Fig. 13. First, Fig. 13b–d shows comparable axial strains in the steel bars at column-footing interface in all studied cases and almost equal to the steel strain in the conventionally reinforced column. Second, the distribution of steel axial strains would be higher than those of the case A (perfect bond) up to 50 mm from column base, but above this point all steel strains are somewhat smaller than those of their counterpart values of the case A. Fig. 13e and f show that the increase in the peak bond strength or the decrease in the slip corresponding to the peak bond strength, respectively, could result in an increase in the axial strain in the FRP bars up to a certain height of the FSRC columns. It should be clear in all cases studied (cases 1–14) that the axial strains in FRP bars are lower than their corresponding values in case A. A question is raised here “why column deformability of the studied cases (1–14) could be higher than that of the column with perfect bond conditions for FRP bars?” Answering this question would lead us to check other sources of column deformability such as rigid body rotation of the columns. Zhao et al. [6] and Fahmy et al. [44] addressed that the member end rotation caused by the slip of longitudinal reinforcement have been considered as a second component of the member deformation besides the flexural deformation. Hence, column end rotation has been defined for all cases studied numerically and presented in Fig. 14 in relation with the applied lateral loads. Fig. 14 shows that when the bond between FRP bars and the surrounding concrete was perfect, the resulted column end rotation at failure was very small compared to the other cases. That is, the propagation of steel yielding up to 400 mm from column base with less concentration of steel deformation at the column base could not compensate the reduction in column deformability. In addition, the contribution from column end rotation is small enough to have a considerable effect on column deformability. Consequently, the column failed to attain a comparable drift capacity to that of the conventionally reinforced column. On the other hand, Fig. 14 shows that column end rotation has a considerable contribution to column deformability especially after the achievement of the column peak lateral strength. Before achieving this strength level, the increase in column end rotation is dependent on the bond strength as shown in Fig. 14a. For instance, after yielding of steel bars and at the same level of loading, the decrease in

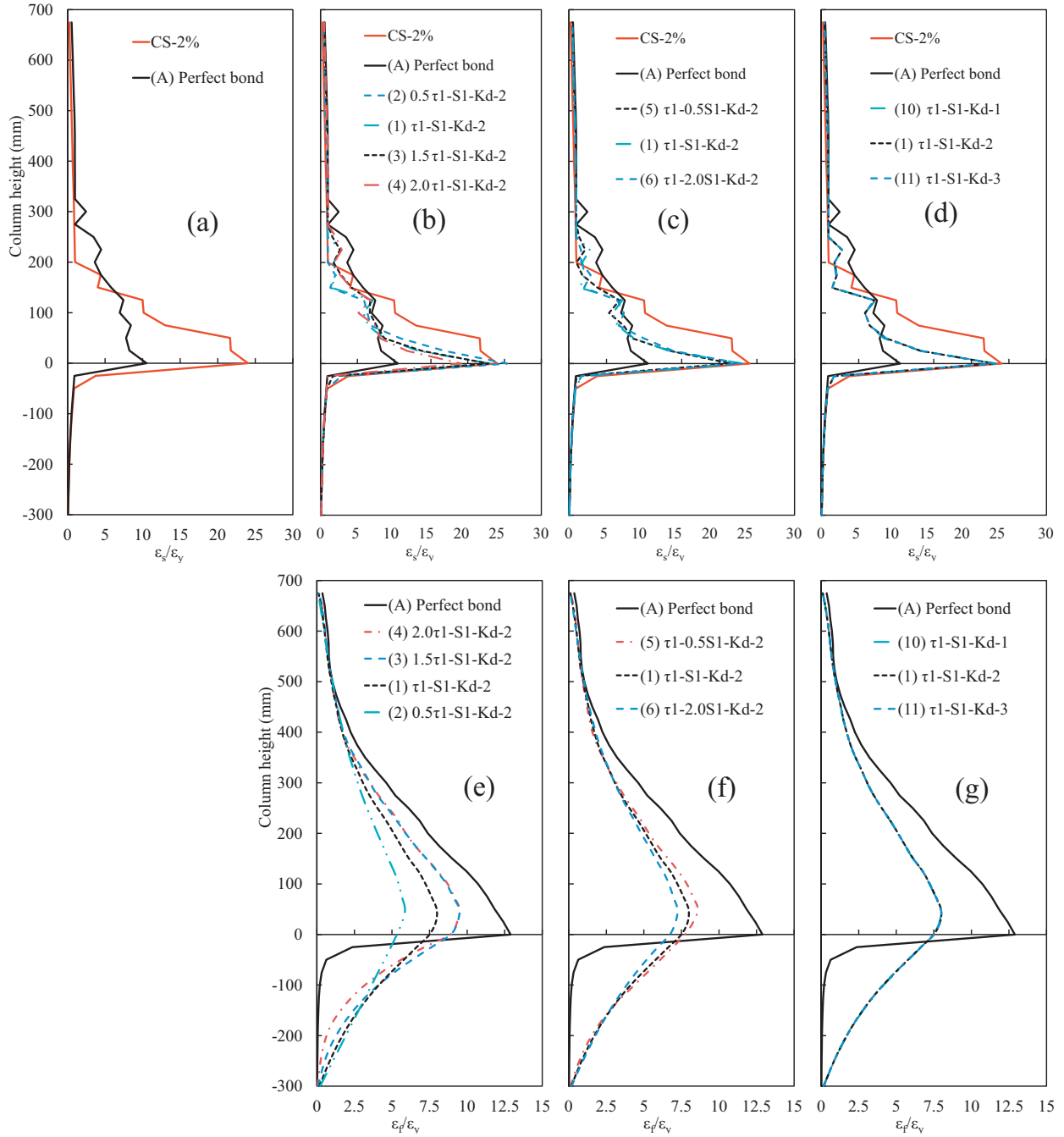


Fig. 13. Steel and FRP strain to yield strain ratio versus column height at lateral drift of 4.2%.

bond strength up to 3.6 MPa shows a considerable increase in column end rotation. As well as, at the column peak lateral strength, it is noticeable that the column end rotation is around 0.007 mm/mm for most cases, and the increase in this value to 0.01 mm/mm could be when slip of the FRP bars at the peak bond strength is 2.2 mm (case 6). A less effect could be noticed for the increase in the slip of FRP bars to 3.3 mm at the end of the plateau zone (case 11), where the column end rotation would increase to 0.0088 mm/mm. Ultimately, Figs. 14b and c show that column end rotation is mostly affected by the slope of the descending branch of the bond–slip relationship of FRP bars. The lower the slope of the descending branch, the higher the column end rotation. Certainly this increase could affect the column deformations only in the ultimate state.

4.4. Probable bond–slip behavior of BFRP bars in FSRC columns assuring ductile-recoverable performance

In the light of the aforementioned experimental and numerical studies on the bond behavior of FRP bars in FSRC columns, results proved the bond-based behavior of the FSRC columns. In fact, the main aim of proposing FRP composites in addition to the conventional reinforcement of RC bridge columns is to achieve the ductile-recoverable performance under the effect of lateral loads. Consequently, definition of a probable bond-conditions between FRP bars and concrete would be very critical to ensure the required structural performance under the effects of lateral loads. Fig.15 presents schematically the sensitivity of the structural performance of the columns to different bond–slip parameters of FRP

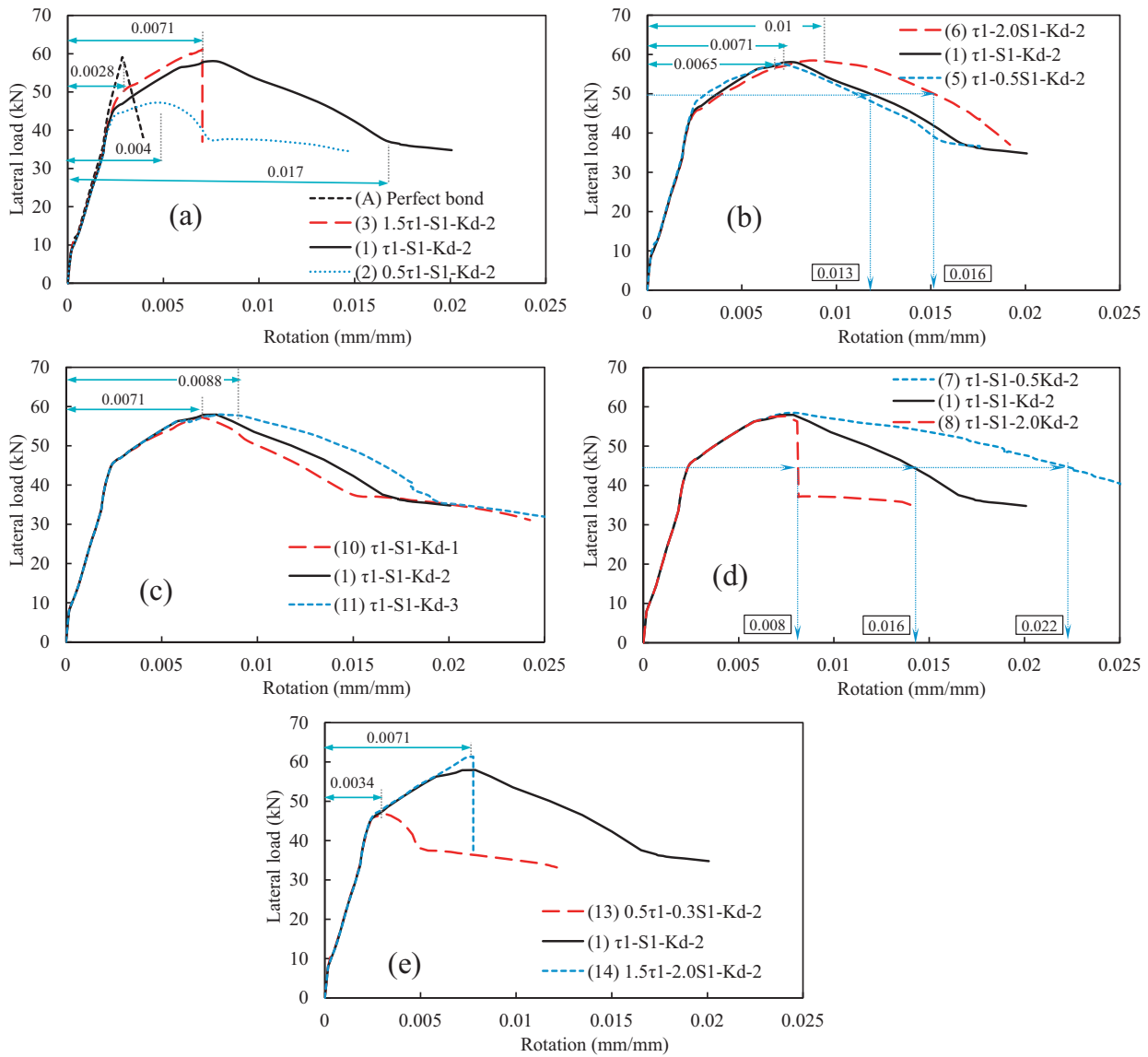


Fig. 14. Column lateral load versus rotation of column-footing interface.

bars based on the results presented in the previous sections. For the serviceability state, yielding load and the corresponding displacement and thus the elastic stiffness (K_1) of FSRC columns are independent on the bond-slip parameters of FRP bars; however, after yielding, the structural performance depends significantly on the bond parameters. In the hardening zone, both the magnitude of post-yield stiffness and the ductility at the lateral strength are directly affected by the bond strength (τ_1) and the corresponding slip (S_1) of FRP bars. In addition, the length of the stability zone depends on both S_1 and length of the horizontal plateau zone (S_2/S_1) of the FRP bond-slip model. Ultimately, the ductility increase in the ultimate state is significantly affected by the fracture energy of the bond-slip model (i.e., the slope of the descending branch, K_d , of the bond-slip model).

Based on the range of bond characteristics considered in the numerical study when concrete compressive strength $f'_c = 30\text{--}40$ MPa, the authors here would recommend the following values for the parameters of bond-slip model to achieve the ductile-recoverable performance under the effect of lateral loads: bond strength should not be less than 7.2 MPa, length of the horizontal plateau zone after the achieved bond strength should be ≥ 3.3 mm, and fracture energy under the descending branch of

the bond-slip relationship should not be less than 80 N/mm. However, comprehensive studies are still required to particularly examine the effect of several potentially influential parameters on the bond behavior of FRP bars to the surrounding concrete and in turn on the damage-controllable state and the ultimate state of FSRC columns. Some of these parameters are linked with both the geometrical and mechanical characteristics of FRP bars and others are dependent on loading type and loading history. Several interesting findings will be presented in future studies by the authors.

5. Summary and conclusions

This paper presented detailed 3D numerical FE modeling of FSRC as well as SRC bridge columns under the effect of combined axial and lateral loads. The structural performance of the FE models was validated in the light of the experimental results of three FSRC columns having BFRP bars with different bond conditions (based on bar texture and bar diameter) as well as one SRC column. All columns were tested under the effect of constant axial load and reversed cyclic loads. In the numerical study, experimental results of pull-out bond tests on BFRP bars of 10-mm diameter embedded in concrete and having different textures were adopted. The

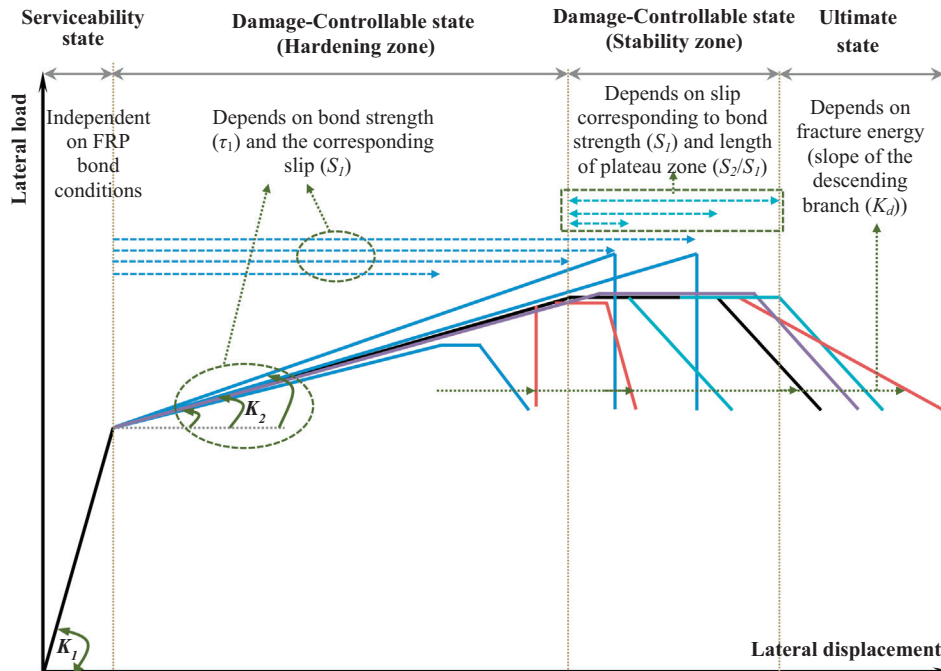


Fig. 15. Schematic figure showing sensitivity of different states of the damage-controlled FSRC column to bond-slip properties of FRP bars under the effect of lateral load.

verified FE model was then employed to investigate the effect of several bond-slip parameters of BFRP bars on the behavior of FSRC columns under the effect of lateral loads. The following conclusions could be drawn:

- (1) Overlooking the bond-slip behavior of FRP bars to the surrounding concrete of FSRC columns could greatly affect the predicted behavior in the post-yielding stages. Compared to the experimental results, the assumption of perfect bond between BFRP bars and the surrounding concrete shows higher stiffening behavior after yielding which is accompanied with underestimation of the column drift capacity due to early rupture of BFRP bars.
- (2) A probable prediction for the behavior of FSRC columns could be recognized when accurate bond-slip models are adopted in the FE simulation for the FRP bars. Macro and micro comparison between experimental results and their counterparts numerically defined (such as lateral load-deformation response, axial strains in steel and FRP bars, and failure mode) showed a good agreement when the real bond conditions between BFRP bars and the surrounding concrete are probably represented in the 3D FE model created.
- (3) Three failure modes were identified from the numerical results: FRP rupture, sudden bond failure and gradual bond-slip failure. FRP rupture is mainly dependent on the bond strength of FRP bars to the surrounding concrete and so bond strength should have a threshold limit to avoid this brittle failure mode; sudden bond failure would take place when slope of the descending branch of bond-slip relationship is quite sharp; and the gradual bond-slip failure is basically based on slip values of FRP bars at the end of the three parts of the bond-slip relationship (ascending, descending, and stabilizing parts).
- (4) All numerically examined bond conditions including perfect bond conditions did not show any clear effect on column elastic stiffness; but, post-yield stiffness, stability zone, and ultimate ductility were very sensitive to bond conditions between FRP bars and concrete: (1) ratio of column post-yield stiffness to the elastic stiffness could be varied between 8.3-to-16.4%; (2) the increase in the displacement ductility, while column strength is constant, could be 0.8-to-3.1; and (3) column ductility at the failure load would show variation from 5.5-to-21.9.
- (5) Lateral strength of the FSRC columns depends mainly on the bond condition of FRP bars to the surrounding materials. Within the range of numerical parametric study, FSRC bridge column reinforced with 0.8% FRP bars and 2% longitudinal steel bars, withstands numerically lateral load varied between 1.25 and 1.75 times the lateral strength of a bridge column reinforced only with 2% longitudinal steel reinforcement based on the values of characteristic parameters of bond-slip relationship of FRP bars used.
- (6) Bond slip models of FRP to concrete with a wider plateau ($S_2 > 3.3$ mm) at the peak bond strength resulted in a longer stability zone at the column's peak strength. Also, the increase in the slip of FRP bars at the peak bond strength has a positive effect on the length of the stability zone compared to the increase in the value of S_2 to 3.3 mm.
- (7) Column end rotation has a considerable contribution to column deformability. The higher the fracture energy of the bond-slip relationship, the higher the column end rotation and in turn the column deformability.
- (8) Numerical as well as experimental findings indicates that characteristics of bond-slip relationship of FRP bars should be adopted as design parameters controlling the behavior of FSRC columns. In the light of the available range of bond-slip results and the experimental results of the cyclic response of FSRC columns, to achieve the aim of continuous increase in column lateral resistance up to high ductility level (>10) with expected reasonable energy dissipation, bond behavior between FRP bars and the surrounding concrete should satisfy the following conditions; bond strength is not less than 7.2 MPa, length of the horizontal plateau zone after the achieved bond strength is ≥ 3.3 mm, and fracture energy under the descending branch of the bond-slip relationship is not less than 80 N/mm.

References

- [1] Focacci F, Nanni A, Bakis CE. Local bond–slip relationship for FRP reinforcement in concrete. *ASCE J Compos Constr* 2000;4(1):24–31.
- [2] Haroun MA, Elsanadedy HM. Behavior of cyclically loaded squat reinforced concrete bridge columns upgraded with advanced composite–material jackets. *J Bridge Eng* 2005;10(6):741–8.
- [3] Niu H, Wu Z. Numerical analysis of debonding mechanisms in FRP-strengthened RC beams. *Comput-Aided Civ Infrastruct Eng* 2005;20(5):354–68.
- [4] Fahmy MFM, Wu ZS, Wu G. Post-earthquake recoverability of existing RC bridge piers retrofitted with FRP composites. *J Constr Building Mater* 2010;24(6):980–98.
- [5] Choi E, Jeon J, Cho B, Park K. External jacket of FRP wire for confining concrete and its advantages. *J Eng Struct* 2013;56:555–66.
- [6] Zhao J, Sritharan S. Modeling of strain penetration effects in fiber-based analysis of reinforced concrete structures. *ACI Struct J* 2007;104(2):133–41.
- [7] Murcia-Delso J, Stavridis A, Shing B. Modeling the bond–slip behavior of confined large diameter reinforcing bars. In: III ECCOMAS thematic conference on computational methods in structural dynamics and earthquake engineering; 2011.
- [8] Tighiouart B, Benmokrane B, Gao D. Investigation of bond in concrete member with fiber reinforced polymer (FRP) bars. *Constr Building Mater* 1998;8(12):453–62.
- [9] Fahmy MFM, Wu Z. Bond-based earthquake-proof of RC bridge columns reinforced with steel rebars and SFCBs. *Earthquake-resistant structures – design, assessment and rehabilitation* 2011; 2012. p. 429–54.
- [10] ACI Committee 408. *Bond and Development of Straight Reinforcing Bars in Tension (ACI408R-03)*, Farmington Hills, Michigan, USA: American Concrete Institute; 2003.
- [11] *Fib. Structural Concrete – Textbook on behaviour, design and performance*, 2nd edition, vol. 1, fib Bulletin 51, fédération internationale du béton, Lausanne; 2009. p. 294.
- [12] Orangin CO, Jirsa JO, Breen JE. A reevaluation of test data on development length and splices. *ACI J Proc* 1977;74(3):114–22.
- [13] Esfahani MR, Rangan BV. Local bond strength of reinforcing bars in normal strength and high-strength concrete (HSC). *ACI Struct J* 1988;95(2):96–106.
- [14] Zuo J, Darwin D. Splice strength of conventional and high relative rib area bars in normal and high-strength concrete. *ACI Struct J* 2000;97(4):630–41.
- [15] Paulay T, Park R, Priestley MJN. Reinforced concrete beam–column joints under seismic actions. *J ACI* 1978;75(11):585–93.
- [16] Tepfers R, De Lorenzis L. Bond of FRP reinforcement in concrete – a challenge. *Mech Compos Mater* 2003;39(4):315–28.
- [17] El Refai A, Ammar M, Masmoudi R. Bond performance of basalt fiber-reinforced polymer bars to concrete". *J Compos Constr* 2015;19(3):04014050.
- [18] Okelo R, Yuan RL. Bond strength of fiber reinforced polymer rebars in normal strength concrete. *ASCE J Compos Constr* 2005;9(3):203–13.
- [19] Aiello MA, Leone M, Pecce M. Bond performances of FRP rebars-reinforced concrete. *J Mater Civ Eng* 2007;19(3):205–13.
- [20] Ammar MA. Bond durability of basalt fibre-reinforced polymers (BFRP) bars under freeze-and-thaw conditions [Thesis, Master of Science], Québec, Canada; 2014.
- [21] Lin X, Zhang YX. Evaluation of bond stress–slip models for FRP reinforcing bars in concrete. *J Compos Struct* 2014;107(37):131–41.
- [22] Hamad B, Rteil A, Soudki K. Bond strength of tension lap splices in high-strength concrete beams strengthened with glass fiber reinforced polymer wraps. *ASCE J Compos Constr* 2004;8(1):14–21.
- [23] Achillides Z, Pilakoutas K. Bond behavior of fiber reinforced polymer bars under direct pullout conditions. *ASCE J Compos Constr* 2004;8(2):173–81.
- [24] Baena M, Torres L, Turon A, Barris C. Experimental study of bond behavior between concrete and FRP bars using a pullout test. *Compos Part B: Eng* 2009;40(8):784–97.
- [25] Cosenza E, Manfredi G, Realfonzo R. Behavior and modeling of bond of FRP rebars to concrete. *ASCE J Compos Constr* 1997;1(2):40–51.
- [26] Hao Q, Wangb Y, He Z, Ou J. Bond strength of glass fiber reinforced polymer ribbed rebars in normal strength concrete. *J Constr Building Mater* 2009;23(2):865–71.
- [27] ElGawady M, Sha'lan A. Seismic behavior of self-centering precast segmental bridge bents. *J Bridge Eng* 2011;16(3):328–39.
- [28] Iemura H, Takahashi Y, Sogabe N. Two-level seismic design method using post-yield stiffness and its application to unbonded bar reinforced concrete piers. *Struct Eng/Earthquake Eng* 2006;23(1):109s–16s.
- [29] Kwan W, Billington SL. Unbonded posttensioned concrete bridge piers. I: monotonic and cyclic analyses. *J Bridge Eng* 2003;8(2):92–101.
- [30] Saiidi MS, O'Brien M, Zadeh MS. Cyclic response of concrete bridge columns using super elastic nitinol and bendable concrete. *ACI Struct J* 2009;106(1):69–77.
- [31] Wu ZS, Fahmy MFM, Wu G. Safety enhancement of urban structures with structural recoverability and controllability. *J Earthquake Tsunami* 2009;3(3):143–74.
- [32] Ibrahim AMA, Wu Z, Fahmy MFM, Kamal D. Experimental study on cyclic response of concrete bridge columns reinforced by steel and basalt FRP reinforcements. *ASCE J Compos Constr* 2015. CC.1943-5614.0000614, 04015062.
- [33] ANSYS User's Manual, Release 13.0. ANSYS, INC., Canonsburg, Pennsylvania; 2010.
- [34] Ibrahim AMA, Fahmy MFM, Wu Z. Numerical simulation on fracturing bond mechanisms of different basalt FRP bars. *JSCE J Applied Mechanics* 2015;71(2):L289–98.
- [35] Elgehausen R, Popov EP, Bertero VV. *Local bond stress–slip relationships of deformed bars under generalized excitations*. Report No. UCB/EERC-83/23, Berkeley, California, USA: University of California; 1983.
- [36] Sato Y, Ko H. Modeling of reinforcement buckling in RC columns confined with FRP. *J Adv Concrete Technol* 2008;6(1):195–204.
- [37] Wolanski JA. *Flexural behavior of reinforced and prestressed concrete beams using finite element analysis*. M. Sov. Diss. Milwaukee, Wisconsin, USA: Marquette University; 2004.
- [38] MacGregor JG. *Reinforced concrete mechanics and design*. Englewood Cliffs, NJ: Prentice-Hall Inc; 1992.
- [39] ACI 318. *Building code requirement for structural concrete (ACI 318-11) and commentary*. Farmington Hills, USA: American Concrete Institute; 2011.
- [40] William KJ, Warnke ED. *Constitutive model for the triaxial behaviour of concrete*. Proceedings of the international association for bridge and structural engineering, 19. Bergamo, Italy: ISMES; 1975. p. 174.
- [41] Kachlakev D, Miller T, Yim S. *Finite element modeling of reinforced concrete structures strengthened with FRP laminates*. Oregon Dept. of Transp., USA, Res. Group, Final Report SPR, 316; 2001.
- [42] CEB. 1992. *CEB-FIP Model Code 90*. London
- [43] Wehbe NI, Saiidi MS, Sanders DH. Seismic performance of rectangular bridge columns with moderate confinement. *ACI Struct J* 1999;96(2):248–58.
- [44] Fahmy MFM, Wu ZS, Wu G, Sun Z. Post-yield stiffnesses and residual deformations of RC bridge columns reinforced with ordinary rebars and steel fiber composite bars. *J Eng Struct* 2010;32(9):2969–83.